ARTICLES
https://doi.org/10.1038/s41477-021-00951-9
nature plants

Check for updates

A species-specific functional module controls formation of pollen apertures

Byung Ha Lee[1,4], Rui Wang[1,4], Ingrid M. Moberg[1,2], Sarah H. Reeder[1], Prativa Amom[1], Michelle H. Tan[1], Katelyn Amstutz[1], Pallavi Chandna[1], Adam Helton[1], Ekaterina P. Andrianova[3], Igor B. Zhulin[3] and Anna A. Dobritsa[1]✉

Pollen apertures are an interesting model for the formation of specialized plasma-membrane domains. The plant-specific protein INP1 serves as a key aperture factor in such distantly related species as *Arabidopsis*, rice and maize. Although INP1 orthologues probably play similar roles throughout flowering plants, they show substantial sequence divergence and often cannot substitute for each other, suggesting that INP1 might require species-specific partners. Here, we present a new aperture factor, INP2, which satisfies the criteria for being a species-specific partner for INP1. Both INP proteins display similar structural features, including the plant-specific DOG1 domain, similar patterns of expression and mutant phenotypes, as well as signs of co-evolution. These proteins interact with each other in a species-specific manner and can restore apertures in a heterologous system when both are expressed but not when expressed individually. Our findings suggest that the INP proteins form a species-specific functional module that underlies formation of pollen apertures.

Pollen grains of flowering plants are surrounded by a robust wall, called exine. In most species, exine is deposited on the pollen surface non-uniformly, with certain regions of the surface receiving little to no exine material[1]. These regions develop into pollen apertures that help pollen to hydrate, change volume and germinate[2–6]. Across species, apertures vary greatly in their number, positions and morphology, contributing to diverse, species-specific patterns on the pollen surface[1,2,7,8]. Recently, we and others have demonstrated that before forming apertures, developing pollen forms distinct aperture domains in their plasma membrane, which accumulate specific combinations of proteins and lipids[6,9–11]. Apertures can thus be used to study how cells develop polarity and form membrane domains, as well as to understand how these mechanisms evolved to create the tremendous diversity of aperture patterns found in nature.

Aperture domains of the plasma membrane appear at the tetrad stage of pollen development, during which the four products of male meiosis (microspores) are transiently kept together under the common callose wall[6,10]. The positions, number and morphology of the aperture membrane domains in microspores correspond to the aperture pattern of mature pollen. For example, in *Arabidopsis* pollen, apertures are shaped like three long and narrow meridional furrows (Fig. 1a). Accordingly, in *Arabidopsis* tetrads, each microspore develops three linear meridional domains of the plasma membrane, which attract the proteins D6 PROTEIN KINASE-LIKE3 (D6PKL3) and INAPERTURATE POLLEN1 (INP1)[10,11]. In contrast, in rice and other grasses, pollen has only one small round aperture, positioned at the distal pole. Correspondingly, the tetrad-stage microspores in rice develop at their distal poles a single aperture domain shaped like a tiny ring, which attracts the rice orthologue of INP1 (OsINP1)[6].

In both *Arabidopsis* and rice, as well as in maize, the INP1 protein was shown to be a major aperture factor whose loss causes a complete loss of apertures (Fig. 1b)[6,9,12]. INP1 is a plant-specific protein with a single recognizable domain, the DELAYED IN GERMINATION1 (DOG1) domain, whose function is unknown[9]. Although the biochemical function of INP1 remains to be identified, in both *Arabidopsis* and rice these proteins appear to play a role in keeping the aperture domains of the plasma membrane in close contact with the overlying callose wall[6,10], which possibly protects these domains from the deposition of exine materials.

Since the role of INP1 as an essential aperture factor is conserved in such distantly related species as *Arabidopsis*, rice and maize, it is reasonable to assume that INP1 orthologues across angiosperms are probably all involved in aperture formation. Intriguingly, though, many INP1 proteins show substantial sequence divergence and cannot substitute for the loss of *Arabidopsis* INP1 (refs. [9,12]). This suggests that, despite their conserved involvement in aperture formation, INP1 proteins are probably functionally species-specific. We have previously proposed that such species specificity might be due to the presence of unknown aperture factors that have co-evolved with INP1 and help it to perform its function[12].

Here, we present an aperture factor, INP2, that fulfills the role of a species-specific partner for INP1. INP2 resembles INP1 in its protein structure, patterns of expression, trends of evolutionary divergence, mutant phenotype and genetic interactions. We provide evidence that INP2 is also functionally species-specific and that it physically interacts with INP1. Furthermore, we demonstrate that tomato orthologues of INP1 and INP2, which are unable to restore apertures in *Arabidopsis* mutants when only one of them is expressed, gain the ability to function in *Arabidopsis* when expressed together. The two INP proteins, therefore, behave as co-evolved species-specific partners that form a functional module required for the formation of pollen apertures.

[1]Department of Molecular Genetics and Center for Applied Plant Sciences, Ohio State University, Columbus, OH, USA. [2]Norwegian Science and Technology University, Ålesund, Norway. [3]Department of Microbiology, Ohio State University, Columbus, OH, USA. [4]These authors contributed equally: Byung Ha Lee, Rui Wang. ✉e-mail: dobritsa.1@osu.edu

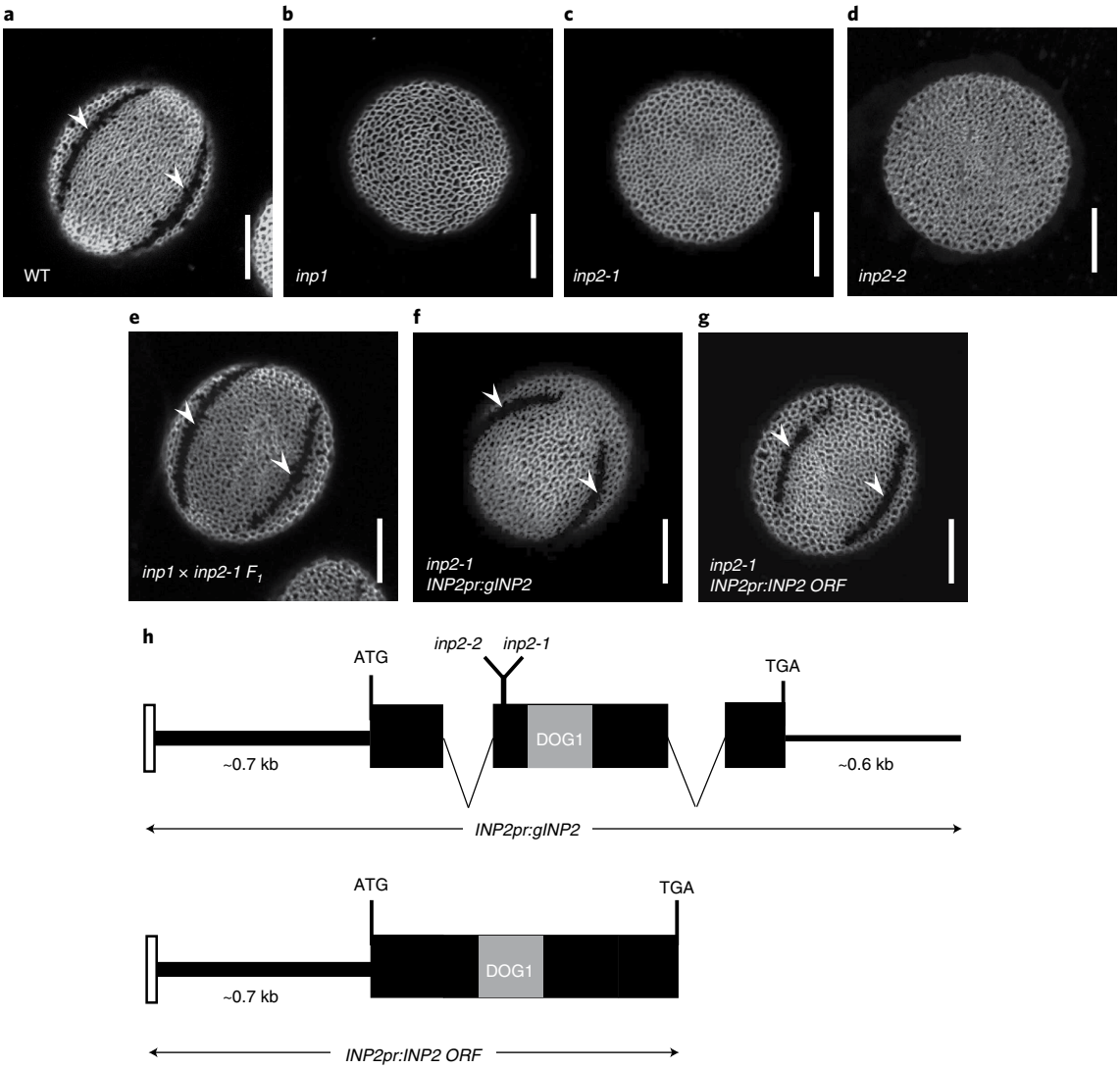

Fig. 1 | *INP2* is a new factor essential for the formation of pollen apertures. a–g, Confocal images of pollen grains stained with auramine O. Scale bars, 10 µm. **a**, Wild-type (WT) *Arabidopsis* pollen has three equidistant furrow-like apertures (two are visible here, arrowheads). **b**, *inp1* pollen completely lacks apertures. **c**,**d**, Similar to *inp1*, pollen of *inp2-1* (**c**) and *inp2-2* (**d**) mutants has normal exine but completely lacks apertures (>100 pollen grains were imaged, with similar results; for *inp2-2*, two independent CRISPR plants were obtained, producing similar phenotypes). **e**, Pollen of the F_1 progeny of the cross between *inp1* and *inp2* develops normal apertures (arrowheads), indicating that mutations disrupt different genes (eight plants (≥50 pollen grains per plant) were imaged, with similar results). **f**,**g**, *INP2pr:gINP2* (**f**) and *INP2pr:INP2 ORF* (**g**) transgenes restore apertures (arrowheads) in *inp2* (7/8 and 15/15 independent T_1 lines, respectively; ≥ 50 pollen grains per line were imaged, with similar results). **h**, *INP2* gene model and structure of the *INP2pr:gINP2* and *INP2pr:INP2 ORF* complementation constructs. Black boxes indicate the protein-coding sequence of At1g15320. The region encoding the DOG1 domain is indicated by the grey box. The white box denotes a short region from the preceding gene, At1g15330, which was included in the constructs. Both the ~0.7-kb upstream region and the ~0.6-kb downstream region were included in the genomic construct. Positions of the *inp2-1* and *inp2-2* mutations are indicated on the gene model.

Results

A new *Arabidopsis* mutant has the inaperturate pollen phenotype identical to the phenotype of the *inp1* mutant. To discover genes involved in the formation of pollen apertures, we performed a forward genetic screen on an M_2 population of *Arabidopsis* plants mutagenized with ethyl methanesulfonate. Since changes in pollen shape can serve as a proxy for aperture formation defects[13,14], we screened these plants for unusual pollen shapes under dissecting microscopes. One mutant produced pollen that looked much rounder than the wild-type pollen, strongly resembling the phenotype of the *inp1* mutants. An examination by confocal microscopy showed that, like *inp1*, pollen of this mutant completely lacks apertures (inaperturate phenotype) but had otherwise normal exine (Fig. 1c).

To test whether the mutation represented an allele of *INP1* or disrupted another gene, we crossed the new mutant with the *inp1-1* null mutant. In the F_1 progeny of this cross, all pollen had normal apertures (Fig. 1e), demonstrating that the defect affected a gene other than *INP1*. This result also showed that, similar to *inp1* and other previously discovered aperture mutants, the new mutation affected a gene with the sporophytic function. Because of the similarities with the *inp1* mutant, we named the new gene *INAPERTURATE POLLEN2 (INP2)* and its mutant allele *inp2-1*.

The *inp2-1* mutation disrupts the At1g15320 gene. Using positional cloning, we mapped the *inp2-1* defect to a 146-kilobase (kb) region at the top of chromosome 1, containing 51 genes. To

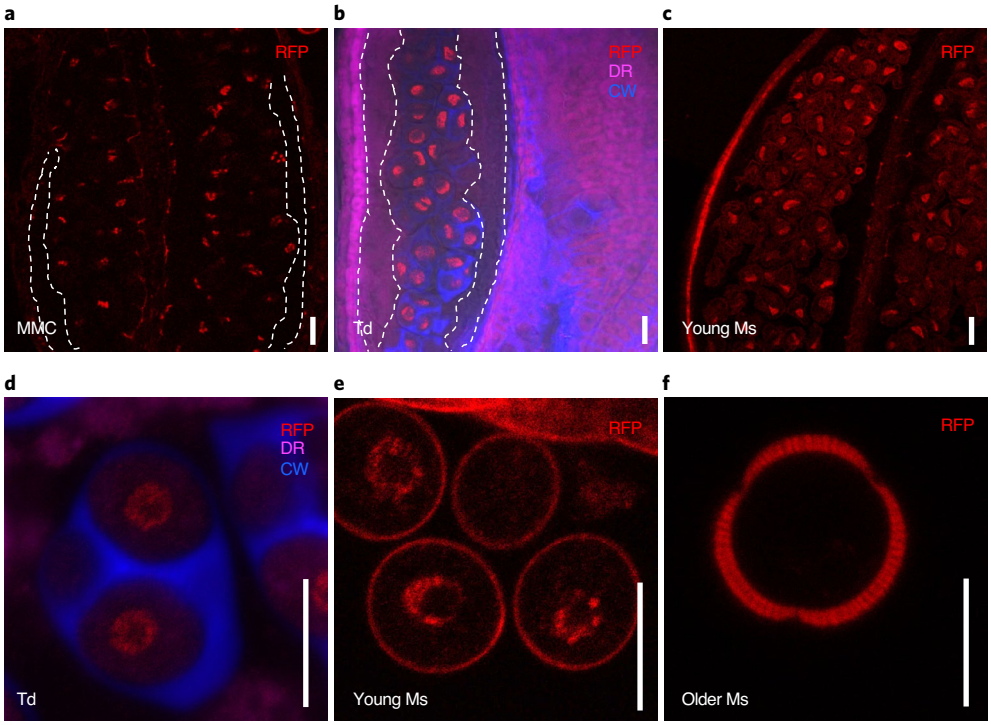

Fig. 2 | *INP2* is expressed in the male reproductive lineage at the time of aperture formation. Images of anthers at different developmental stages (**a–c**) and magnified images of the cells from the male reproductive lineage at different developmental stages (**d–f**) expressing the transcriptional fusion construct *INP2pr:H2B-RFP*. Nuclear signal of H2B-RFP (red) is found in dividing microspore mother cells (MMC; **a**), tetrads of microspores (Td; **b**,**d**) and young free microspores (Ms; **c**,**e**). Older microspores (**f**) do not show nuclear H2B-RFP signal (peripheral red signal is due to the autofluorescence of the developing exine). No signal was observed in the tapetal layer of the anther (outlined by the white dashed lines in **a**,**b**). Besides RFP, the images in **b**,**d** show staining for callose wall (blue, CW, calcofluor white) and membranous structures (magenta, DR, CellMask Deep Red). Five independent T_1 lines were imaged, with similar results. Scale bars, 10 μm.

narrow down the list of gene candidates, we inspected their predicted identities as well as patterns of their messenger RNA expression reported in the TRAVA RNA-seq database[15]. We focused on the genes expressed in young flower buds (flowers 12–18 in the TRAVA nomenclature), as these buds include the tetrad stage of development associated with aperture formation. One gene, At1g15320, was prioritized as a particularly strong candidate as it is predicted to be expressed nearly exclusively in young buds (Extended Data Fig. 1) and encodes a protein with structural similarities to INP1 (below). Sequencing of this gene from *inp2-1* revealed a G-to-A substitution which created an early stop codon (Trp84Stop) (Fig. 1h). To independently confirm that *INP2* is At1g15320, we targeted At1g15320 in the wild-type Col-0 background with CRISPR-Cas9 and generated an allele (*inp2-2*) with a two-nucleotide deletion that caused a frame shift after the amino acid 83 (Fig. 1h). The CRISPR mutant displayed the same inaperturate pollen phenotype as the original *inp2-1* allele (Fig. 1d).

To further verify the identity of At1g15320 as *INP2* and to define its regulatory regions, we created transgenic constructs containing either the genomic region of At1g15320 (including introns and the ~0.6-kb region downstream of the stop codon) or its open reading frame (ORF) (Fig. 1h). These constructs were placed under the control of the putative native promoter (a region of ~0.7-kb between the start codon of At1g15320 and the preceding gene At1g15330) and transformed into *inp2-1*. Both constructs successfully restored apertures in transgenic plants—15/15 T_1 plants with the ORF construct and 7/8 T_1 plants with the genomic construct (Fig. 1f–g). Taken together, our results demonstrate that (1) At1g15320 encodes INP2 (a new factor essential for aperture formation) and (2) that the 0.7-kb upstream region is sufficient to drive functional expression of *INP2*. This promoter region was then used for all subsequent *INP2* constructs transformed into *Arabidopsis*.

INP2 shares structural similarity with INP1. INP2 is a plant-specific protein of unknown biochemical function which shares certain similarities with INP1. Both proteins have similar size (273 amino acids for INP1 versus 307 amino acids for INP2), are usually encoded in angiosperm genomes by single-copy genes and contain the same domain—the plant-specific DELAYED IN GERMINATION1 (DOG1) domain (PFam14144) (Fig. 1 and Extended Data Fig. 2a). This domain, typically associated with seed dormancy proteins and TGA bZIP transcription factors[16], is the only recognizable domain in both INP proteins. Interestingly, although INP1 and INP2 share only limited homology with each other (23% sequence identity; Extended Data Fig. 2a), the protein-fold recognition software Phyre2 (ref. [17]) selected the same template for homology modeling of both proteins and predicted similar structures, with three alpha-helices, for their C-terminal regions (Extended Data Fig. 2b,c).

Protein alignments of INP1 and INP2 with their respective orthologues from other plants also revealed that, in eudicots, these proteins typically contain a region enriched in Asp and Glu residues. However, these acidic regions are positioned differently between INP1 and INP2. In the INP1 proteins, the acidic region follows the DOG1 domain[9,12], whereas in the INP2 proteins it is located ahead of the DOG1 domain (Extended Data Fig. 3).

For *Arabidopsis thaliana* INP2 (AtINP2), multiple algorithms also predicted the existence of a transmembrane (TM) domain at its N terminus (Extended Data Fig. 4), with most of the protein expected to be outside the cell, facing the extracellular space. Yet,

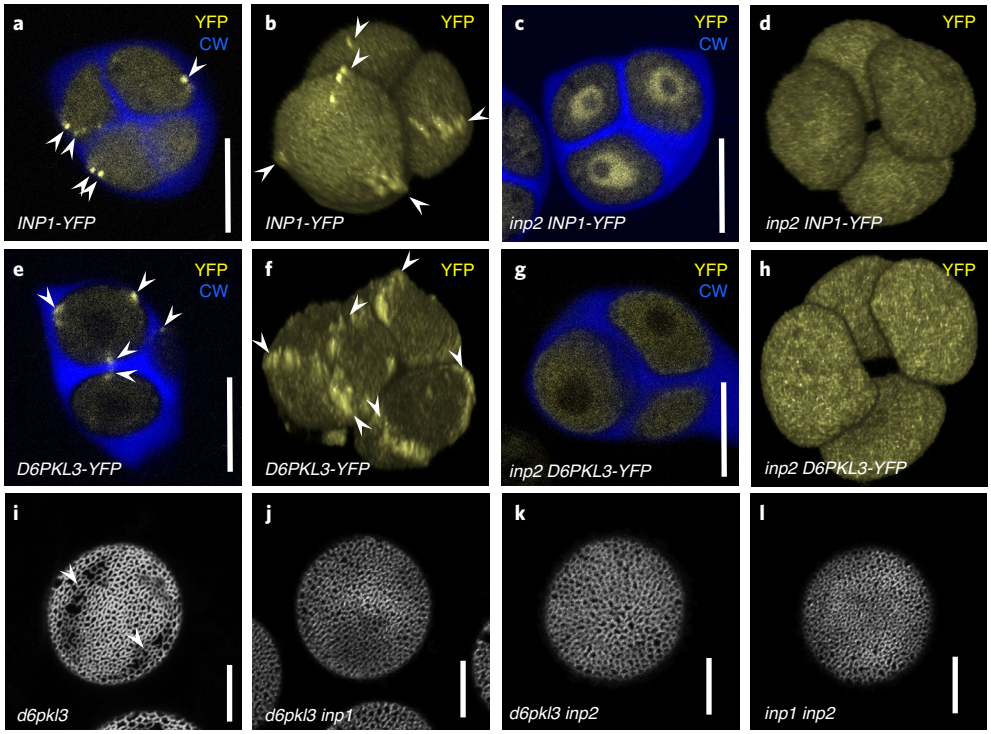

Fig. 3 | INP2 is required for INP1 and D6PKL3 accumulation at the aperture domains and both *inp1* and *inp2* are epistatic to *d6pkl3*. **a**–**h**, INP1-YFP and D6PKL3-YFP localization in tetrads of microspores in the presence and absence of INP2. Confocal optical sections (**a**,**c**,**e** and **g**) and three-dimensional reconstructions of tetrads of microspores (**b**,**d**,**f** and **h**). YFP signal is shown in yellow and callose wall (CW, stained by calcofluor white) is shown in blue. Arrowheads point to the YFP signal at the aperture domains. INP1-YFP localizes to the aperture PM domains in the wild type (**a**,**b**) but loses this localization in the *inp2* mutant (**c**,**d**), instead becoming enriched in the nucleoplasm. Experiments in (**c**,**d**) were repeated three times, with similar results. Likewise, D6PKL3-YFP localizes to the aperture domains in the wild type (**e**,**f**) but loses this localization in the *inp2* mutant (**g**,**h**). Experiments in **g**,**h** were repeated two times, with similar results. **i**–**l**, *inp1* and *inp2* mutations are epistatic to *d6pkl3* and do not cause additional phenotypic changes when combined. Confocal images of pollen grains stained with auramine O. The *d6pkl3* mutant pollen often develops apertures partially covered with exine (arrowheads) (**i**), whereas double mutants *d6pkl3 inp1* (**j**), *d6pkl3 inp2* (**k**) and *inp1 inp2* (**l**) completely lack apertures. Three or more plants (≥50 pollen grains per plant) were imaged in **i**–**l**, with similar results. Scale bars, 10 μm.

the algorithms failed to identify a TM domain in many orthologues of AtINP2, including the highly related proteins from *A. lyrata* and other members of the Brassicaceae family, suggesting that this is not a common feature of INP2 proteins. No lipid modifications are predicted for INP2.

INP2 is expressed in the developmental lineage of pollen at the time of aperture formation. Publicly available RNA-seq data show that, like INP1, INP2 is expressed nearly exclusively in young buds containing pollen at or around the tetrad stage during which apertures form (Extended Data Fig. 1). To test whether in these buds INP2 is expressed in the male reproductive lineage, we expressed the nuclear marker histone H2B tagged with red fluorescent protein (RFP) under the control of the *INP2* promoter (*INP2pr:H2B-RFP*) in the wild-type Col-0 plants. This reporter, with its concentrated localization in the nucleus, was specifically chosen to help visualize the expression from the *INP2* promoter, since, like *INP1*, *INP2* is predicted to be expressed at low levels (Extended Data Fig. 1). The nuclear RFP signal was found in the dividing microspore mother cells, tetrad-stage microspores and young free microspores (Fig. 2). The signal was absent in older microspores, the surrounding somatic tapetal cell layer and other

Fig. 4 | INP1 and INP2 physically interact. **a**, Yeast two-hybrid assay of interaction between INP1 and INP2$^{\Delta N}$ (lacking the N-terminal region). BD, DNA-binding domain; AD, activating domain; SD, synthetic defined medium. To test for the presence of both BD and AD constructs, leucine (L) and tryptophan (W) were excluded from the medium. To test for protein interaction, yeast were grown on media lacking L, W and histidine (H) and containing 20 mM 3-aminotriazole (3-AT). **b**, BiFC experiments. INP1 and INP2 proteins fused, respectively, to the N- and C-terminal parts of YFP (YN and YC) were cotransformed into tobacco leaves to test for interaction. Cotransformation of INP1-YN with only YC and cotransformation of INP2-YC with only YN were used as negative controls. Top panels show YFP signal in leaf epidermis. Bottom panels show merged YFP and bright-field images. Scale bars, 50 μm. **c**, Co-immunoprecipitation experiments. INP1-HA_3/INP2-GFP and INP1-GFP/INP2-HA_3 pairs (or just single tagged proteins as negative controls) were co-expressed in tobacco leaves, precipitated with anti-GFP and visualized with anti-GFP or anti-HA. IP, immunoprecipitation; IB, immunoblot. 'Mock' indicates protein extract from leaves infiltrated only with buffer. **d**, Split-luciferase assay. Tobacco leaves were divided into sectors co-expressing indicated proteins containing the N-terminal (NLuc) and C-terminal (CLuc) parts of the firefly luciferase. Panels on the left show the bright-field images and panels on the right show the corresponding luminescence images. **e**, Y2H assay in which the DOG1 domains of INP1 (INP1^{DOG1}) and INP2 (INP2^{DOG1}) were tested for interaction with each other, self-interaction and interaction with the full-length INP1 and with INP2$^{\Delta N}$. The description is the same as for **a**, except that 3 mM 3-AT was used here. Experiments in **a**–**c** and **e** were repeated three times and experiments in **d** were repeated two times (each time using multiple leaves from multiple plants), with similar results.

anther layers (Fig. 2). This expression pattern matches that of INP1 (refs. [9,10]).

To visualize the subcellular localization of the INP2 protein, we first created five constructs, in which INP2 was tagged with yellow fluorescent protein (YFP) at four positions: at the N terminus, at the C terminus (either directly or following an 18-amino acid linker), after the predicted TM region and internally—within the low-conservation region (below). However, none of the YFP-tagged constructs rescued the *inp2* mutant, suggesting that INP2 does not tolerate addition of sizable tags. This notion was supported by further experiments in which partial rescue of the mutant phenotype was achieved with constructs expressing INP2 tagged at the C terminus with one or three copies of the small HA tag. Of these two types of constructs, the shorter HA_1 construct produced better rescue (Methods), yet no protein signal was detected in these lines with anti-HA in anther sections or whole-mount preparations, possibly owing to the low levels of the INP2 expression. This prevented us from determining whether INP2, like INP1, specifically localizes to the aperture domains in the plasma membrane of microspores.

Localization of INP1 and D6PKL3 to plasma-membrane aperture domains depends on the presence of INP2. To test whether INP2

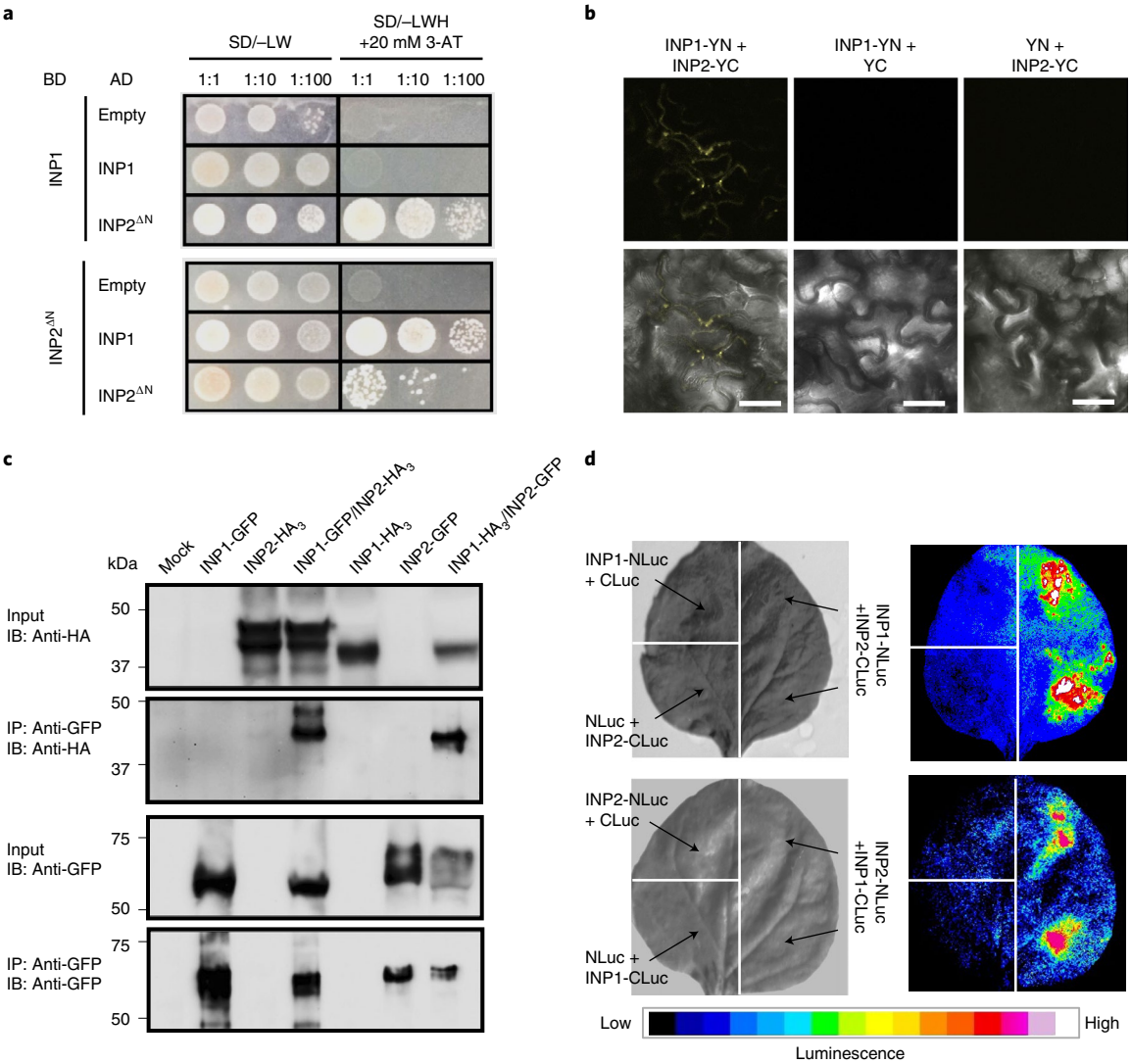

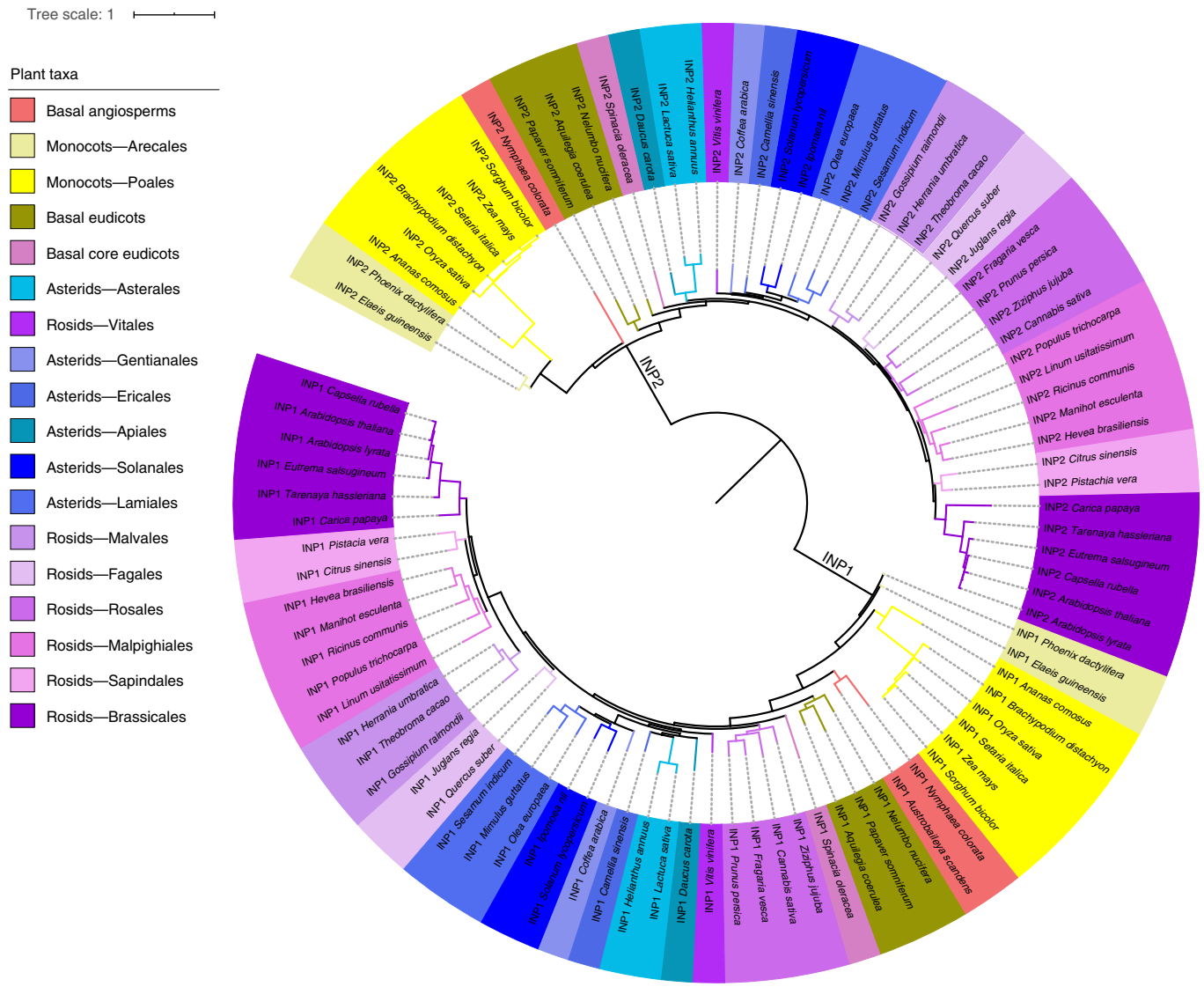

Fig. 5 | INP1 and INP2 exhibit similar trends of evolutionary sequence divergence. Maximum likelihood phylogenetic tree of INP1 and INP2 sequences from a variety of angiosperm taxa (indicated by colour coding). The INP1 and INP2 sequences cluster into two separate clades, which display similar topology.

contributes to the distinct positioning of INP1 and another recently identified aperture factor, D6PKL3, both of which accumulate at the microspore aperture domains (Fig. 3a,b,e,f), we introgressed the previously characterized reporter constructs *DMC1pr:INP1-YFP* (ref. [10]) and D6PKL3*pr*:D6PKL3-*YFP* (ref. [11]) into the *inp2* mutant background. In the absence of INP2, INP1-YFP failed to localize to the aperture domains of the plasma membrane, instead showing notable enrichment in the nucleoplasm (Fig. 3c,d). This result suggests that INP2 is involved either in targeting INP1 to the aperture domains or in keeping it there. Likewise, in the absence of INP2, the membrane-associated kinase D6PKL3-YFP lost its association with the aperture domains, instead displaying diffuse cytoplasmic localization (Fig. 3g,h). As D6PKL3 reacts the same way to the absence of INP1 (ref. [11]), both INP1 and INP2 are thus required to keep it at the aperture domains.

To test for epistatic relationships between these aperture factors, we created double mutants of *inp1 d6pkl3* and *inp2 d6pkl3*. Single mutations in D6PKL3 do not completely abolish aperture formation, instead producing 'shadows of apertures' that are partially covered with exine (Fig. 3i)[11]. Yet both double mutants produced completely inaperturate pollen (Fig. 3j,k), indicating that *inp1* and *inp2* are both epistatic to *d6pkl3*. To investigate the possibility of synergistic interactions between *INP1* and *INP2*, we also created the *inp1 inp2* double mutant. Its phenotype, however, was identical to those of single mutants (Fig. 3l), showing that the simultaneous loss of INP1 and INP2 does not cause any additional observable effects (for example, in the exine deposition) and suggesting that these proteins behave as bona fide aperture factors. Taken together, the results presented so far are consistent with the notion that INP1 and INP2 occupy very similar positions in the aperture formation pathway and might coordinate their activities.

INP1 and INP2 are interacting proteins. Since INP1 and INP2 exhibit similarities in their protein structures, patterns of expression, mutant phenotypes and genetic interactions, we suggested that they might physically interact. To explore this possibility, we used several approaches. An initial yeast two-hybrid (Y2H) assay with the full-length INP1 and INP2 did not result in yeast growth

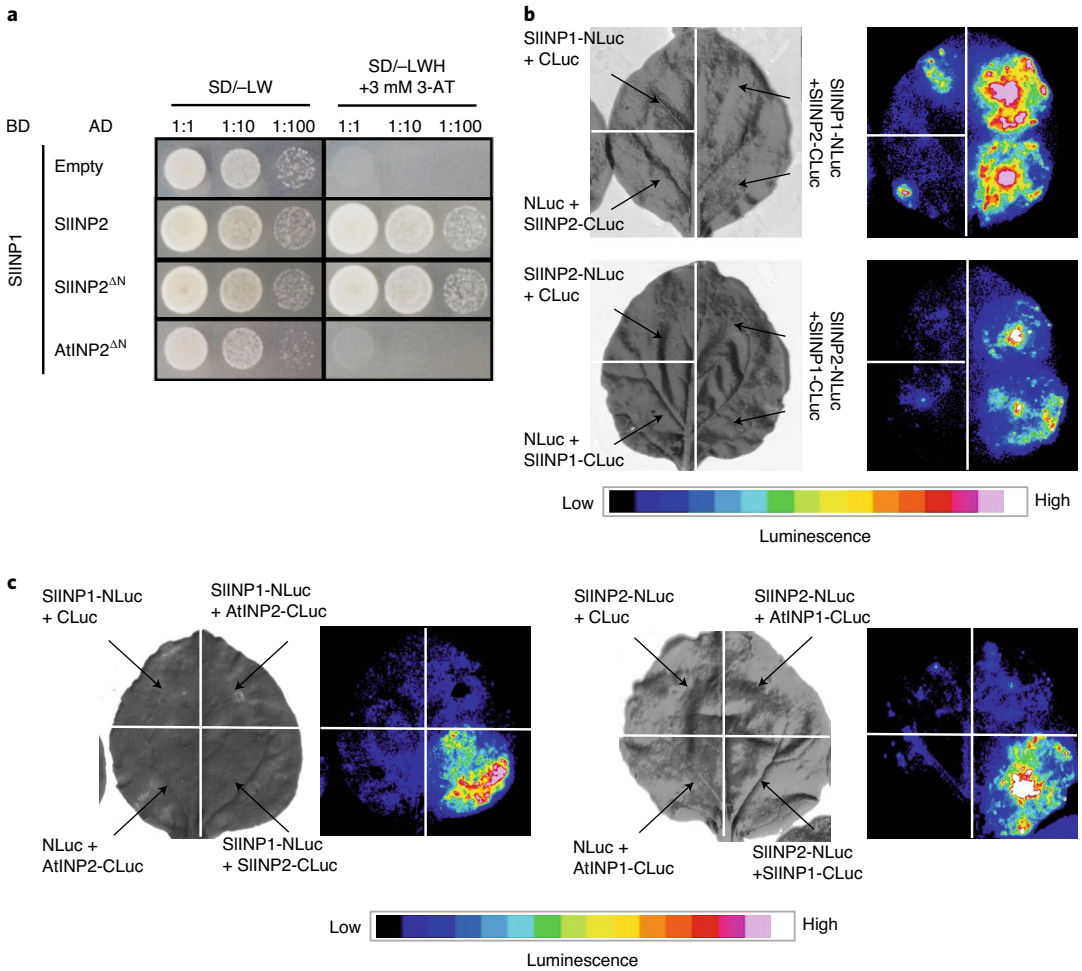

Fig. 6 | INP1 and INP2 interact in a species-specific manner. a, Y2H assay testing SlINP1 interactions with SlINP2 (or SlINP2$^{\Delta N}$ lacking the N-terminal region) and AtINP2$^{\Delta N}$. To test for the presence of both BD and AD constructs, leucine (L) and tryptophan (W) were excluded from the medium. To test for protein interaction, yeast were grown on media lacking L, W and histidine (H) and containing 3 mM 3-aminotriazole (3-AT). **b**, Split-luciferase assay testing the ability of SlINP1 and SlINP2 to interact. Tobacco leaves were divided into sectors co-expressing indicated proteins containing the N-terminal (NLuc) and C-terminal (CLuc) parts of the firefly luciferase. Panels on the left show the bright-field images and panels on the right show the corresponding luminescence images. **c**, Split-luciferase assay testing the ability of INP1 and INP2 from *Arabidopsis* and tomato to interact with a protein from another species. Only the same-species interactions were observed. The description is the same as for **b**. All experiments were repeated at least twice, with similar results.

indicative of protein interaction. We reasoned, however, that lack of yeast growth would be expected if INP2 indeed had a TM domain at its N terminus and most of the protein was extracellular.

We, therefore, expressed INP2 in yeast without its first 24 amino acids, which contained the predicted TM domain. This truncated INP2 (INP2$^{\Delta N}$) showed strong interaction with INP1 in the Y2H system (Fig. 4a). In addition, this assay revealed that INP2 may be able to self-interact (Fig. 4a). We further verified the ability of INP1 and INP2 to interact in planta by expressing them in tobacco leaf cells and performing co-immunoprecipitation, bifluorescent molecular complementation (BiFC) and a split-luciferase assay (Fig. 4b–d).

The DOG1 domain is the only recognizable protein domain present in these proteins. Although its function is unknown, it has been proposed that this domain might participate in protein–protein interactions[18]. We therefore used the Y2H assay to test the ability of the DOG1 domains from INP1 and INP2 to interact with each other and with the full-length (or nearly full-length in the case of INP2$^{\Delta N}$) proteins (Fig. 4e). INP1^{DOG1} was able to interact with INP2$^{\Delta N}$. In contrast, INP2^{DOG1} failed to interact with INP1 but showed some ability to interact with INP2$^{\Delta N}$, consistent with the finding that INP2 may self-interact. However, no interactions occurred when only the DOG1 domains were present (Fig. 4e), suggesting that these regions probably interact with other portions of INP2.

INP1 and INP2 exhibit similar trends of evolutionary sequence divergence. We previously reported that INP1 greatly diversified in angiosperm lineages[9,12]. Still, in several species these divergent orthologues were found to be involved in the formation of pollen apertures and able to localize to specific plasma-membrane aperture domains[6,12], suggesting that, despite the substantial difference in primary sequences, all INP1 proteins in angiosperms probably function as aperture factors. However, INP1 proteins appear to exhibit a notable degree of functional species specificity, since the divergent INP1 orthologues were not able to complement the aperture defects of the *Arabidopsis inp1* mutant[12]. A possible interpretation of this result is that INP1 proteins might require the presence of co-evolved partners to perform their function.

To see whether INP2 shows signs of co-evolution with INP1, we performed BLAST searches for INP2 homologues followed by phylogenetic analysis, revealing notable parallels between INP1 and INP2. Although proteins with the DOG1 domain appeared as

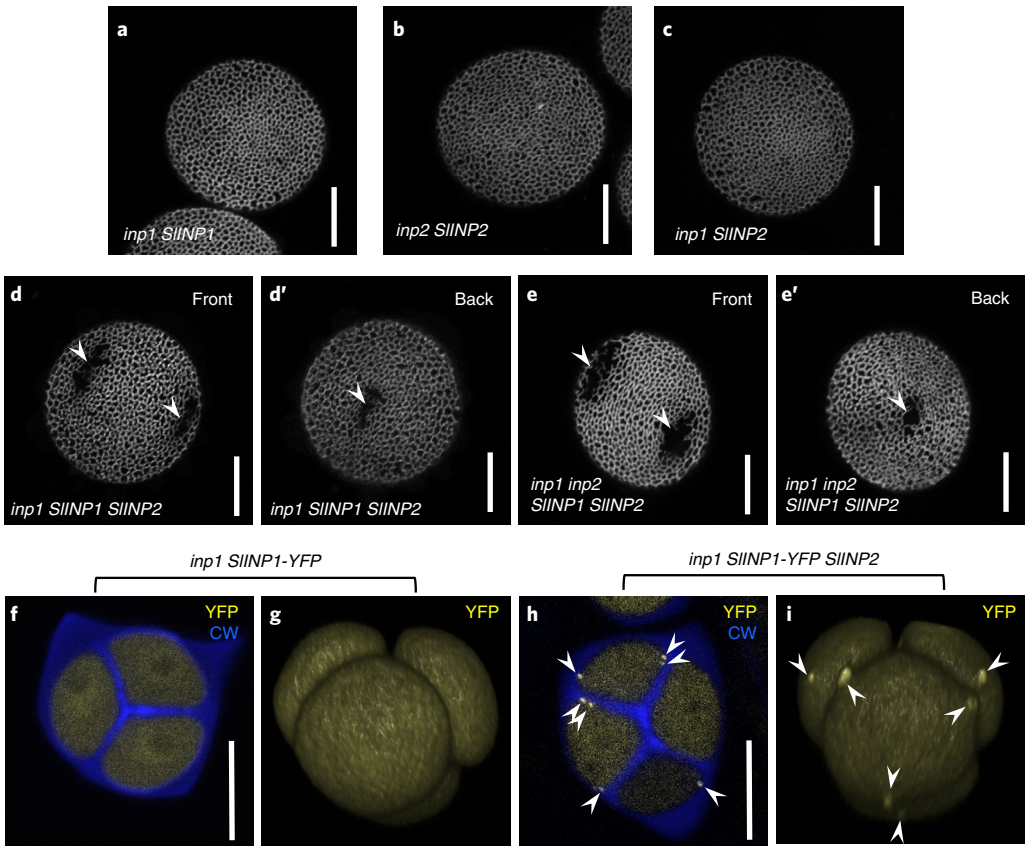

Fig. 7 | Tomato orthologues of INP1 and INP2 fail to function in *Arabidopsis* when expressed individually but gain this ability when co-expressed. **a–c**, Neither SlINP1 (**a**) nor SlINP2 (**b**,**c**) are able to restore apertures in *Arabidopsis* pollen when expressed on their own. More than ten T_1 plants (≥ 50 pollen grains per plant) were analysed, with similar results. **d**–**e′**, When both SlINP1 and SlINP2 are expressed in *Arabidopsis*, they restore short to medium apertures (arrowheads) in the *inp1* (**d**,**d′**) and *inp1inp2* (**e**,**e′**) *Arabidopsis* mutants. Confocal images of pollen grains stained with auramine O. Both front and back views are shown for the same pollen grains in (**d**,**d′**) and (**e**,**e′**) to demonstrate positions of apertures. Experiments were repeated twice, with similar results (~90% of plants had short- to medium-size apertures and the rest had no apertures). **f**–**i**, SlINP1-YFP localizes to the aperture domains in the presence of SlINP2 (**h**,**i**) but not when expressed on its own (**f**,**g**). Confocal optical sections (**f**,**h**) and three-dimensional reconstructions of tetrads of microspores (**g**,**i**). YFP signal is shown in yellow and callose wall (CW, stained by calcofluor white) is shown in blue. Arrowheads point to the YFP signal at the aperture domains. Experiments were repeated twice, with similar results. Scale bars, 10 μm.

early as green algae, we found distinct, well-supported INP1 and INP2 protein lineages only in gymnosperms and angiosperms. In angiosperms, they have greatly diversified and display similar trends of evolutionary divergence, resulting in phylogenetic trees of similar topology (Fig. 5). Orthologues of both INP1 and INP2 exist in various families of rosids, asterids, basal eudicots, monocots and magnoliids. The INP1 sequence is also present among the transcripts from two ANA-grade basal angiosperms, Austrobaileya and Nymphaea. Failure to find an INP2 homologue in Austrobaileya, despite finding one in Nymphaea, could be due to the incompleteness of the database. Interestingly, both INP1 and INP2 are absent from the genome of *Amborella*, another basal angiosperm whose genome was published several years ago[19].

Degrees of sequence divergence within the INP1 and INP2 angiosperm lineages are generally consistent with the phylogenetic relationships between species (Supplementary Table 1 and Fig. 5). Both *Arabidopsis* INP1 and INP2 (AtINP1 and AtINP2) share between ~95 and ~70% protein sequence identity with their respective orthologues from closely related species in the Brassicaceae and Cleomaceae families. Sequence identity with orthologues from more distantly related eudicots drops to ~40–50%. In monocots, the similarities to AtINP1 and AtINP2 are further reduced: proteins from Arecaceae and Bromeliaceae families (for example, palms and pineapple) exhibit ~45 to ~30% sequence identity with AtINP1 and AtINP2. In both INP1 and INP2 lineages, particularly distinct clades are formed by proteins from grasses (Poaceae) (Fig. 5 and Supplementary Table 1): within each INP group, these proteins diverged greatly from the rest of their lineages (showing ~35 and ~20–25% identity, respectively, to AtINP1 and AtINP2) but retained >80% identity to their orthologues from other species of Poaceae despite the long evolutionary history of this monocot family[20].

INP1 and INP2 are functionally species-specific. The similar evolutionary trends displayed by INP1 and INP2, as well as the ability of these proteins to interact, led us to suggest that INP2 might serve as a species-specific partner for INP1. We tested this idea using the orthologues of INP1 and INP2 from tomato *Solanum lycopersicum* (SlINP1 and SlINP2) which both share ~45% amino acid identity with their *Arabidopsis* counterparts. Using the Y2H and split-luciferase assays, we confirmed the ability of SlINP1 and SlINP2 to interact (Fig. 6a,b). Furthermore, in both assays, the tomato INP proteins specifically interacted with each other and not with the *Arabidopsis* proteins (Fig. 6a,c).

We demonstrated previously that SlINP1 was unable to localize to aperture domains and restore apertures when expressed in the *Arabidopsis inp1* mutant[12] (Fig. 7a). Here, we placed *SlINP2*

under the control of the *AtINP2* promoter and transformed the *AtINP2pr:SlINP2* construct into the *Arabidopsis inp2-1* mutant. Similar to SlINP1, SlINP2 failed to restore apertures in the *Arabidopsis inp2* mutant (12/12 T_1 plants; Fig. 7b), suggesting that INP2 probably also exhibits functional species specificity.

Co-expression of SlINP1 and SlINP2 restores aperture formation in *Arabidopsis* mutants. Since individually expressed SlINP1 and SlINP2 did not restore apertures in *Arabidopsis* (Fig. 7a,b), we tested if together they could gain functionality in that species. To this end, we transformed *INP2pr:SlINP2* into *inp1* (as expected, apertures were not restored in all 14 T_1 plants; Fig. 7c) and crossed these plants with the previously characterized *DMC1pr:SlINP1-YFP inp1* transgenic lines[12]. In the resulting *inp1* progeny that inherited just a single transgene, no apertures were restored. But, remarkably, among the *inp1* progeny that inherited both transgenes, 91% of plants (64/70) produced pollen with short- to medium-size apertures (Fig. 7d,d′).

Because SlINP1 was tagged with YFP, we assessed its localization in *Arabidopsis* tetrad-stage microspores. As shown previously[12], when expressed on its own, SlINP1-YFP fails to accumulate at the plasma-membrane aperture domains, instead localizing diffusely in the cytoplasm (Fig. 7f,g). However, in the presence of SlINP2, SlINP1-YFP gained the ability to successfully assemble into distinct puncta at the plasma-membrane aperture domains (Fig. 7h,i).

We further crossed the *SlINP1 SlINP2 inp1* plants with *inp2* plants to generate the double *inp1 inp2* mutants carrying both transgenes. In the F_2 and F_3 generations, those double mutants that inherited both tomato transgenes also produced pollen with apertures (Fig. 7e,e′). Taken together, these results demonstrate that SlINP1 and SlINP2 act as species-specific partners in pollen aperture formation.

Certain regions of INP2 mediate its species specificity in *Arabidopsis*. To identify sequences in INP2 responsible for the species specificity of this protein, we divided it into seven regions, on the basis of position relative to the transmembrane and DOG1 domains and evolutionary conservation (Fig. 8a and Extended Data Fig. 3). Regions were chosen as follows: (1) the N terminus (N), which in AtINP2 encompasses the predicted TM region; (2) the acidic region, which, besides its enrichment in Asp and Glu residues, is fairly divergent across species; (3) the middle region; (4) the DOG1 domain; (5) the low-conservation region (LCR), which shows high sequence divergence across species; (6) the conserved C-terminal region (CTR); and (7) the highly divergent C-tail. To test which of the AtINP2 regions were necessary for its function, we created seven chimaeric transgenic constructs in which most of the sequence came from AtINP2, while one region at a time was replaced with the corresponding sequence from SlINP2 (Fig. 8a). In addition, to test if any of the AtINP2 regions were sufficient for its function in *Arabidopsis*, we created a complementary set of seven constructs; in those, most of the protein was from SlINP2 and a single region came from AtINP2 (Fig. 8a). These 14 constructs were transformed into the *Arabidopsis inp2* mutant and their ability to complement the mutant phenotype was assessed.

The AtINP2 constructs in which the N terminus, the middle region, the LCR or the CTR were replaced with the SlINP2 sequences all restored apertures in *Arabidopsis* (19/19, 10/12, 10/12, 19/20 T_1 plants, respectively) (Fig. 8a,b,d,f,g), indicating that AtINP2 can tolerate the presence of tomato sequences in these four regions. The ability of the construct with the Sl N terminus to function in *Arabidopsis* was surprising, as this region in SlINP2 is not predicted to contain a TM domain.

In contrast, the AtINP2 constructs with the SlINP2 acidic region or the DOG1 domain failed to rescue apertures in *Arabidopsis* (Fig. 8a,c,e) (11/11 T_1 plants for both constructs), demonstrating that these regions are critical for species-specific interactions. In addition, although five out of 12 T_1 plants expressing AtINP2 with the tomato C-tail had some ability to produce short apertures (Fig. 8h), overall, the $AtINP2^{SlC\text{-}tail}$ protein performed poorly: in ten out of 12 T_1 plants all or some pollen grains lacked apertures (Fig. 8h'). The divergent C-tail, therefore, probably also contributes to the protein's species specificity.

The complementary set of the SlINP2 constructs with single AtINP2 regions showed that none of the AtINP2 regions was sufficient on its own to convert SlINP2 into a protein able to function in *Arabidopsis* (Fig. 8a and Extended Data Fig. 5; ten or more T_1 plants were analysed for each construct). This suggests that sequences from more than one region contribute to the INP2 species specificity.

We then explored the extent to which AtINP2 can tolerate the simultaneous replacement of the regions which, individually, did not impact its functionality. The chimaeric INP2s in which either the N terminus and the middle region or the LCR and the CTR came from SlINP2 were still functional in *Arabidopsis* (Fig. 8a,i,j; 16/18 T_1 plants for $AtINP2^{SlN+mid}$ and 18/18 T_1 plants for $AtINP2^{SlLCR+CTR}$). In contrast, the simultaneous replacement of the middle region and the CTR ($AtINP2^{Slmid+CTR}$) resulted in a pronounced loss of protein activity: pollen developed either only very short apertures and 'shadows of apertures' (Fig. 8a,k; 10/17 T_1 plants) or no apertures at all (7/17 T_1 plants). The replacement of all four of these regions ($AtINP2^{SlN+mid+LCR+CTR}$) resulted in a completely non-functional protein (Fig. 8a,l; 13/13 T_1 plants), indicating that while each of these four regions plays a less prominent role in the species-specific functionality of INP2 compared to the acidic region, the DOG1 domain and the C-tail region, together they still provide important contributions.

Discussion

The diversity of pollen aperture patterns in nature probably reflects the diversity of mechanisms controlling formation of these structures. In this study, we identified and characterized the new pollen aperture factor INP2, which is essential for this process and acts as a species-specific partner for the previously discovered aperture factor INP1. While not closely related, INP1 and INP2 share multiple similarities, including their matching patterns of expression, identical mutant phenotypes and the presence of the DOG1 domain (Figs. 1–3). Phylogenetic analysis suggests that the two *INP* genes are the result of an ancient gene duplication that occurred in the common ancestor of gymnosperms and angiosperms, with the diverging genes evolving non-redundant functions important for the formation of pollen apertures. INP1 and INP2 proteins interact with each other, display similar evolutionary trends and show functional species specificity (Figs. 4–7), indicating that they have co-evolved to form a species-specific functional module that promotes aperture formation. The notion of species specificity of the components of this module is strongly supported by the ability of the tomato SlINP1 and SlINP2 proteins to restore apertures in *Arabidopsis* only when

Fig. 8 | Certain regions of INP2 mediate its species specificity. a, A diagram of 18 *INP2* chimaeric constructs containing regions from *Arabidopsis* (At, green) and tomato (Sl, magenta). The protein was divided into seven regions. The ability of a construct to restore apertures in the *Arabidopsis inp2* mutant is indicated by '+', the failure to restore apertures is indicated by '−' and the ability to restore apertures in some but not all transgenic lines is indicated by '+/−'. **b**–**m**, Representative images of pollen grains produced by transgenic *inp2* plants expressing different chimaeric *INP2* constructs. Over ten independent T_1 lines were tested for each construct (≥50 pollen grains per line), with all or nearly all lines producing similar results, except in **h**, **h'** and **k** where, as described, some plants produced short apertures and others no apertures. Apertures are indicated by arrowheads. Scale bars, 10 μm.

they are co-expressed but not when expressed individually (Fig. 7). We have also demonstrated that SlINP1, which, on its own, does not assemble at the aperture domains in *Arabidopsis* tetrads[12], gains the ability to do this in the presence of SlINP2 (Fig. 7h,i). Our data show that several regions of INP2, including the DOG1 domain, contribute to its species specificity (Fig. 8).

a

Construct	N	Acidic	Middle	DOG1	LCR	CTR	C-tail	Rescue
AtINP2$^{Sl\ N}$	Sl	At						+
AtINP2$^{Sl\ acid}$	At	Sl	At					–
AtINP2$^{Sl\ mid}$	At		Sl	At				+
AtINP2$^{Sl\ DOG1}$	At			Sl	At			–
AtINP2$^{Sl\ LCR}$	At				Sl	At		+
AtINP2$^{Sl\ CTR}$	At					Sl	At	+
AtINP2$^{Sl\ C\text{-}tail}$	At						Sl	+/–
SlINP2$^{At\ N}$	At	Sl						–
SlINP2$^{At\ acid}$	Sl	At	Sl					–
SlINP2$^{At\ mid}$	Sl		At	Sl				–
SlINP2$^{At\ DOG1}$	Sl			At	Sl			–
SlINP2$^{At\ LCR}$	Sl				At	Sl		–
SlINP2$^{At\ CTR}$	Sl					At	Sl	–
SlINP2$^{At\ C\text{-}tail}$	Sl						At	–
AtINP2$^{Sl\ N\ +\ mid}$	Sl	At	Sl	At				+
AtINP2$^{Sl\ LCR\ +\ CTR}$	At				Sl	At		+
AtINP2$^{Sl\ mid\ +\ CTR}$	At		Sl	At		Sl	At	+/–
AtINP2$^{SlN\ +\ mid\ +\ LCR\ +\ CTR}$	Sl	At	Sl	At	Sl		At	–

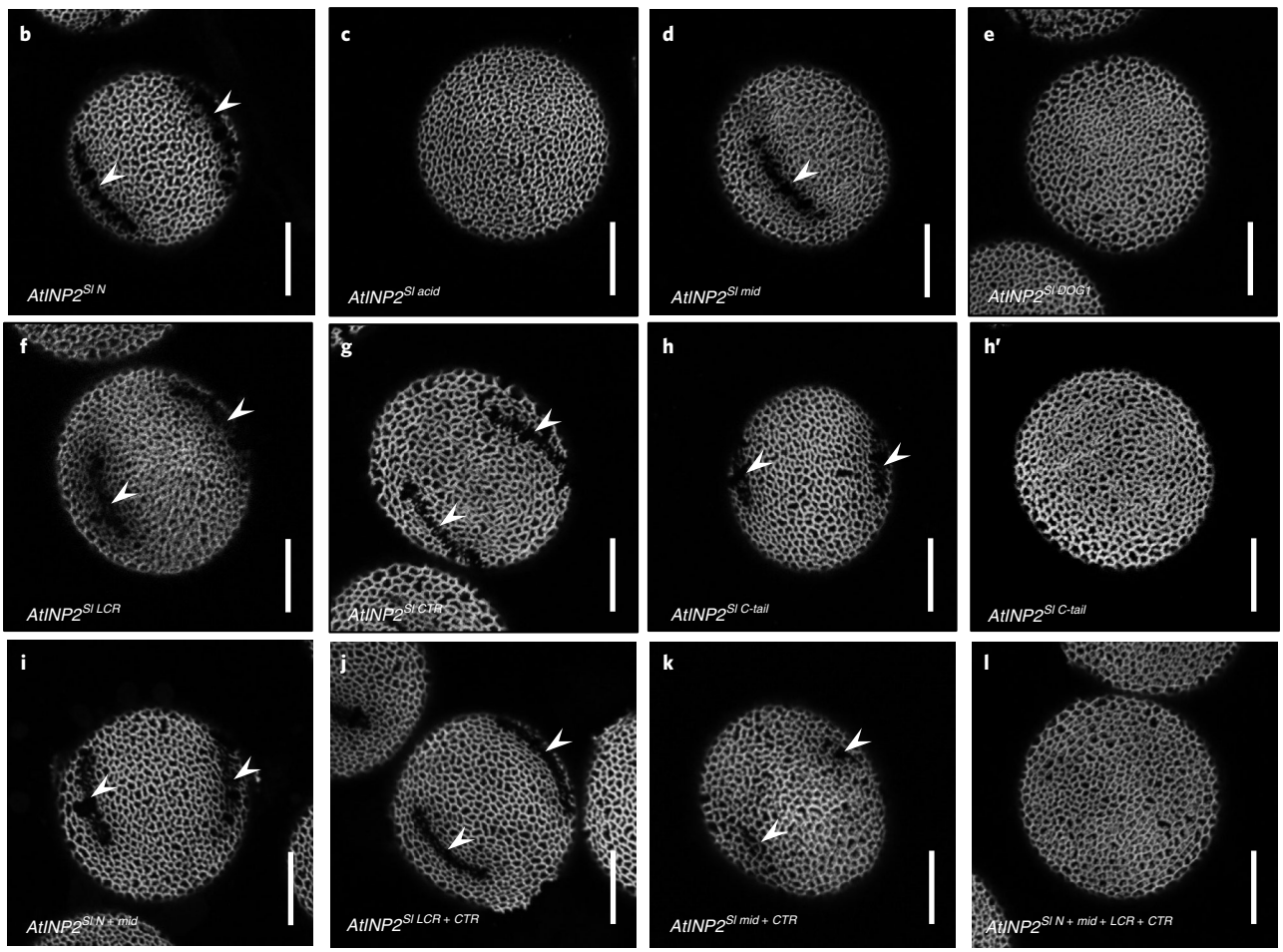

INP1 and INP2 are both proteins of unknown function. Accumulating evidence for the *Arabidopsis* INP1 indicates that it is a late-acting aperture factor that becomes attracted to the plasma-membrane domains in microspores that are already pre-specified as aperture sites[12,14,21]. As such, even though INP1 and its partner INP2 are critical for aperture formation, they are unlikely to directly define positions and morphology of apertures and to contribute to the aperture diversity in that way. This idea is supported by the phenotype of the apertures restored in the *Arabidopsis inp1* mutant by the expression of the tomato SlINP1/SlINP2 complex: the restored apertures did not resemble the colporate tomato apertures (PalDat: www.paldat.org)[8,12] but were more like the colpate apertures of *Arabidopsis* (Fig. 7d,e′). It is, therefore, intriguing why these essential, yet late-acting aperture factors have diversified so much among angiosperms. This could indicate that different species have variations in the upstream mechanisms or differences in other interactors of the INP proteins. Relevant to this point, the apertures restored by the tomato complex in *Arabidopsis* were shorter than the normal *Arabidopsis* (or tomato) apertures (Fig. 7d,e′). While this could be due to reduced expression of the transgenes compared to that of endogenous genes, an alternative possibility is that, for optimal function, the tomato complex requires some additional species-specific component(s).

After aggregating at the aperture domains, the INP1 proteins in both *Arabidopsis* and rice participate in keeping the plasma membrane at these domains near the overlying callose wall and preventing the deposition of the exine precursor, primexine, at these sites[6,10]. How can the newly discovered INP2 protein contribute to aperture formation? There are several possibilities and further investigations will be needed to distinguish between them. For instance, along with INP1, INP2 might directly be a part of the protein complex that assembles at the aperture domains and mediates their interaction with the callose wall. Alternatively, INP2 might be involved in the delivery of INP1 to its positions at the aperture domains. AtINP1 appears to aggregate on the extracellular side of the aperture domains, yet lacks a clear signal peptide or any obvious means to become anchored at the plasma membrane[10]. The proposed topology of AtINP2, with the TM domain at its N terminus and most of the protein outside the cell, is consistent with the idea that the INP1/INP2 complex in *Arabidopsis* is extracellular. It is tempting to speculate that the interaction of AtINP1 with the extracellular portion of AtINP2 could provide a way to anchor AtINP1 at the aperture domains. Yet, further experimentation will be needed to validate the topologies of AtINP2 and its orthologues from other species, many of which, like SlINP2, lack predicted TM domains; to find a way to visualize the INP2 subcellular localization; and to establish whether the INP proteins from species with very different aperture patterns function in the same way. Intriguingly, OsINP1 from rice was recently shown to interact with the cytoplasmic portion of a lectin receptor-like kinase[6], suggesting a possibility that in grasses, whose single pore-like apertures differ greatly from the three furrows in *Arabidopsis* and tomato, INP1 might have a role at the cytoplasmic side of the aperture domains. Since both INP lineages in grasses have greatly diverged from their counterparts in eudicots and some other monocots, it would be very interesting to determine whether in that plant family INP2 proteins are also involved in aperture formation and function in a complex with INP1 or whether they have evolved other functions.

In conclusion, our study uncovered a new essential player in the poorly understood mechanism underlying the formation of important patterning elements on the pollen surface and demonstrated that the two DOG1 domain-containing aperture factors form a protein complex whose components contribute to the species specificity of this molecular mechanism.

Methods

Plant materials and growth conditions. Plants were grown at 20–22 °C with the 16-h light/8-h dark cycle in growth chambers or in a greenhouse at the Biotechnology facility at Ohio State University (OSU). Besides the genotypes generated in this study, the following genotypes were used: Columbia (Col-0), Landsberg *erecta* (Ler), *inp1-1* (ref. [9]), *DMC1pr:INP1-YFP inp1-1* (refs. [10,14]); *DMC1pr:SlINP1-YFP inp1-1* (ref. [12]); and D6PKL3*pr*:D6PKL3-*YFP d6pkl3-2* (ref. [11]).

Forward genetic screen. The genetic screen which led to the isolation of the *inp2-1* mutant was recently described[21]. In brief, M_2 plants (~10,000) from eight pools of ethylmethane sulfonate-treated lines of Ler background were screened for the presence of morphological abnormalities in their pollen (for example, in size, shape, light reflection, ease of pollen release from anthers) identifiable with standard dissecting stereomicroscopes (Zeiss Stemi-2000C and Nikon SMZ745) at 75–80× magnification. Particular attention was paid to changes in pollen shape, known to be associated with aperture defects[9,13]. For primary screening, dry pollen did not undergo any treatment. At this level of magnification, pollen of the *inp2-1* mutant looked rounder than the wild-type pollen. Pollen was then stained with auramine O as described in ref. [14] and aperture defects were observed with confocal microscopy. Mutant *inp2-1* was then backcrossed with Ler once. To test for complementation, *inp2-1* mutant was crossed with *inp1-1* and the pollen of their F_1 progeny was observed with dissecting and confocal microscopes.

Mapping the *inp2* defect. Mutant *inp2-1* with Ler background was crossed with Col-0 and the resulting F_2 population was screened under a dissecting microscope for the presence of the round-pollen mutant phenotype. DNA was isolated from 189 mutants. First, the bulked segregant analysis[22] placed the mutation to the top of chromosome 1. This was followed by map-based positional cloning using individual F_2 mutants[22]. The INDEL-based polymerase chain reaction (PCR) markers for this analysis were generated as previously described[11], using combined information from the 1,001 Genomes Project database (http://signal.salk.edu/atg1001/index.php)[23] and the Arabidopsis Mapping Platform[24]. The mutation was mapped to a 146-kb region between 5,151,424 and 5,297,411 base pairs (bp).

To determine which of the 51 genes in this interval was responsible for the aperture defect in *inp2*, we used information from the *Arabidopsis* RNA-seq database TRAVA (travadb.org)[15] to identify genes expressed in the young buds at or near the tetrad stage of pollen development (flowers 12–18). Although 37 of the 51 genes are expressed in buds at these stages, expression of only one of them, At1g15320, is specifically restricted to these tissues and stages. The finding that this gene, like *INP1*, encodes a protein with the DOG1 domain led us to further prioritize it as a strong candidate for *INP2*. Sequencing of this gene from the *inp2-1* mutant revealed the presence of the point mutation which leads to a premature stop codon (Trp84Stop).

Sequence retrieval and phylogenetic analysis. Sequences of INP1 and INP2 homologues were retrieved by TBLASTN from NCBI (https://blast.ncbi.nlm.nih.gov/Blast.cgi), Phytozome v.12.1 (https://phytozome.jgi.doe.gov/pz/portal.html), the 1000 Plants project (OneKP-China National Gene Bank (https://db.cngb.org/onekp/)[25] and PLAZA (https://bioinformatics.psb.ugent.be/plaza/)[26]. Accession numbers are provided in Supplementary Table 1. For multiple sequences alignment, MAFFT v.7.017 (L-INS-i algorithm) was used. The alignment positions with more than 20% gaps were removed with trimAl[27]. ModelFinder[28] accessed through IQ-TREE[29] tested 546 protein models to find the best-fit model of evolution (INP1 + INP2: JTT + R5). Lastly, the IQ-TREE program[30] was used to construct phylogenetic trees, with the maximum likelihood method and 1,000 bootstrap replicates. The trees were visualized in iTOL v.5 (ref. [31]).

Confocal microscopy. Preparation and imaging of mature pollen and tetrads were performed as previously described[14]. Three-dimensional reconstruction of tetrads was done using NIS Elements v.4.20 software (Nikon).

Generation of the CRISPR allele of *INP2*. The guide RNA for the At1g15320 gene was selected with the help of the CRISPR-PLANT platform (https://www.genome.arizona.edu/crispr/)[32] and its sequence was cloned into the pHEE401E vector[33] as described[34] using primers Oligo-01-F-INP2-T1/Oligo-R-INP2-T1 (Supplementary Table 2). The resulting construct was transformed into the *Agrobacterium tumefaciens* strain GV3101 and *Arabidopsis* Col-0 plants were transformed using the floral dip method[35]. The T_1 transformants were selected on hygromycin plates and 18 seedlings were transferred to soil. Two of the 18 T_1 plants displayed the inaperturate phenotype. Sequencing of the At1g15320 gene from these two plants revealed that both had the same homozygous single-nucleotide deletion which occurred one nucleotide before the PAM sequence and caused a shift in the ORF after the codon 83.

***INP2* complementation and expression constructs.** Primers used in this study are listed in Supplementary Table 2. All fragments for cloning were amplified with high-fidelity Phusion DNA polymerase (NEB, M0530 or Thermo Fisher, F530). To create the *INP2pr:INP2 ORF* construct, the *INP2* promoter (a fragment of 701 bp

from the end of the preceding gene to the start codon of *INP2*) and ORF were amplified, respectively, with primer pairs INP2pr-IF-F/ INP2pr-IF-R and INP2 ORF-IF-F/ INP2-Stop-IF-R from the Col-0 genomic DNA and from the *INP2* complementary DNA clone DQ446252 obtained from the Arabidopsis Biological Resource Center. The resulting two fragments were cloned into the SacI and SpeI sites in the pGR111 binary vector[36] using in-fusion cloning (Takara, no. 638950). A BamHI site was introduced in front of the *INP2* start codon to facilitate subsequent cloning. To create the *INP2pr:gINP2* construct, the genomic fragment, which included the coding sequence, introns and the 567-bp region downstream of the *INP2* stop codon, was amplified from Col-0 genomic DNA with primers INP2 ORF-IF-F/gINP2-SpeI-R and cloned downstream of the *INP2* promoter between the BamHI and SpeI sites. Constructs were verified by sequencing and transformed into the *A. tumefaciens* strain GV3101. The *inp2* plants were then transformed by floral dip. Transgenic T_1 plants were selected with BASTA and the presence of transgenes was confirmed with specific primers.

To generate the reporter construct *INP2pr:H2B-RFP*, the *H2B-RFP* fusion gene was cloned into the BamHI/SpeI sites downstream of the *INP2* promoter in pGR111 and the construct was transformed into the Col-0 plants.

To express INP2 tagged at the C terminus with one or three copies of HA (HA_1 and HA_3), we first used the in vivo assembly (IVA) cloning in *E. coli*[37] to combine the *INP2* ORF (without the stop codon), an eight-amino acid Gly-rich linker (G_5PGS) and the corresponding HA tag in the pGEM-T-Easy vector (Promega). After confirming the sequences, the tagged *INP2* sequences were placed into pGR111 under the control of the *INP2* promoter and the resulting constructs were transformed into *inp2*. The shorter construct with HA_1 produced better rescue. Out of the 14 *INP2-HA*$_1$ T_1 lines, 11 had long to medium-size apertures, two had short apertures and one had no apertures. Out of the 13 *INP2-HA*$_3$ T_1 lines, four had medium-size apertures, four had short apertures and five had no apertures. Note that the construct with HA_3 inserted directly after INP2 (without the Gly-rich linker) essentially failed to rescue the mutant phenotype (2/9 T_1 lines produced short apertures and the rest produced no apertures).

***SlINP1*, *SlINP2* and *Arabidopsis*/tomato chimaeric *INP2* constructs.** The tomato paralogues of *INP1* and *INP2* were identified in the tomato genome, respectively, as Solyc08g079050 and Solyc03g116770. The *DMC1pr:SlINP1-YFP* construct was previously described[12] and the previously characterized transgenic lines of *DMC1pr:SlINP1-YFP inp1* were used in this study. To create the *INP2pr:SlINP2* construct, the tomato genomic DNA was amplified with primers BamHI-SlINP2-BF/SpeI-SlINP2-AR. The resulting fragment was digested with BamHI/SpeI and used to replace the *AtINP2* gene in the *INP2pr:gINP2* construct. The construct was transformed into the *inp2* and *inp1* mutants, transgenic T_1 plants were selected with BASTA and the presence of the transgene was confirmed with specific primers.

To genotype the F_2 populations which segregated both the *DMC1pr:SlINP1-YFP* and *INP2pr:SlINP2* transgenes in combination with the *inp1* or *inp1 inp2* mutations, the following primers and conditions were used: for *SlINP1*, 2-Sl-F/ Sly INP1-R-NcoI primers; for *SlINP2*, AD23/AD8 primers; for *inp1*, a cleaved amplified polymorphism (CAPS) marker was used (22600-DF/22600-DR primers, SacI cuts the mutant allele, digestion products resolved on 1.5% agarose gels); for *inp2*, a derived CAPS (dCAPS) marker was used (At1g15320-BF/AD402 primers, AccI cuts the mutant band, digestion products resolved on 4% agarose gels). PCR with 40 cycles (98 °C for 15 s, 55 °C for 15 s, 72 °C for 30 s) were performed in all cases.

To quickly generate multiple chimaeras of *AtINP2* and *SlINP2*, we used the ORF versions of the constructs and the IVA cloning method[37]. The *AtINP2* ORF was first amplified using primers pGEM-INP2-IF-F/INP2-pGEM-IF-R and cloned with the help of the in-fusion procedure into the pGEM-T-Easy vector digested with SacI and NcoI. A BamHI site and a SpeI site were introduced, respectively, at the beginning and at the end of the *AtINP2* sequence for ease of subsequent subcloning into the binary pGR111 vector. To obtain the *SlINP2* cDNA, total mRNA was isolated from young tomato buds with Trizol (Thermo Fisher, no. 15596026) and converted into cDNA as previously described[14]. The *SlINP2* ORF was then amplified with primers AD19/AD16 and used to replace *AtINP2* between the BamHI and SpeI sites with the help of the IVA method in pGEM-T-Easy vector, which itself was amplified with AD17/AD14 primers. The resulting pGEM-T-Easy-based *AtINP2* and *SlINP2* constructs were used as backbone templates for chimaeras, while pGR111-based constructs were used as the *INP2*-region templates in IVA cloning. Thirty primers (AD1 through AD28, pGEM-INP2-IF-F and INP2-pGEM-IF-R) were used in different combinations (as indicated in Supplementary Table 2) to obtain all 18 chimaeras. IVA reactions were performed as described in ref. [37]: products of single PCR amplified with sets of four primers were treated with DpnI (15 min at 37 °C) to degrade templates and directly transformed into *E. coli*. Single-region chimaeras were used as backbone templates to generate multiregion chimaeras. All chimaeric sequences were verified by sequencing, cut out with the BamHI/SpeI digestion, subcloned downstream of the *INP2* promoter in the pGR111 vector and resequenced again. The final constructs were transformed into the *inp2* mutant; transgenic T_1 plants were selected with BASTA and the presence of the transgenes was confirmed with specific primers.

Yeast two-hybrid assay. The Y2H assays were performed as previously described[11]. The DNA-binding domain construct *pB29-INP1* and the activation-domain construct *pP6-INP1* were described previously[11]. Other constructs were created by cloning the coding sequences of *AtINP2*, *SlINP1*, *SlINP2* or their truncated forms into the same vectors. Constructs were cotransformed in indicated combinations into the NMY51 yeast strain. Positive bait-prey cotransformants were selected on the synthetic dropout medium lacking Leu and Trp (–LW). To test for interaction, cotransformed yeast cells were grown on the medium that lacked Leu, Trp and His and contained either 3 mM or 20 mM 3-amino-1,2,4-triazole (–LWH + 3-AT).

Bifluorescent molecular complementation assay. To create the *35Spr:nYFP-AtINP1* and *35Spr:cYFP-AtINP2* constructs, *AtINP1* and *AtINP2* ORFs were, respectively, amplified with AD17-BHL/AD18-BHL and AD469/470 primers, digested with PacI/XbaI and inserted into *35Spr:nYFP*$_{(1–158)}$ and *35Spr:cYFP*$_{(159–238)}$ binary vectors[38]. Constructs were transformed into *A. tumefaciens* strain GV3101. Bacterial cultures containing these constructs were grown to optical density $OD_{600} = 0.4$ and co-infiltrated into tobacco (*Nicotiana benthamiana*) leaves along with agrobacteria expressing the RNA silencing suppressor P19 (ref. [39]) at the 1:1:2 ratio. Infiltrated leaves were grown for 5 d, after which samples were collected and imaged on a Nikon A1 + confocal microscope using identical settings for all imaging. Samples were excited with a 514-nm laser and YFP emission was collected at 522–555 nm.

Co-immunoprecipitation. AtINP1 and AtINP2 ORFs were amplified through two sequential PCR reactions (first PCR with primers AD326/488 for AtINP1 and primers AD370/489 for AtINP2; second PCR with primers AD122/123 for both genes) and inserted into the pDONR207 vector through the Gateway BP recombination reaction (Invitrogen, no. 11789020). Gateway LR recombination reaction was then used to transfer these sequences into the pCsVMV:GFP-C-999 or pCsVMV:HA-C-1300 vectors[40] (a gift from D. Somers, OSU), producing four constructs: CsVMV-AtINP1-GFP, CsVMV-AtINP1-HA3, CsVMV-AtINP2-GFP and CsVMV-AtINP2-HA3. All constructs were verified by sequencing and transformed into the *A. tumefaciens* strain GV3101 by electroporation. Tobacco leaves were infiltrated with different combinations of constructs (as described for BiFC above), harvested 5 d after infiltration and stored at −80 °C for at least 1 d. A total 1 µl of monoclonal anti-GFP (A-11120, Molecular Probes by Thermo Fisher Scientific) was incubated with 1 µl of protein A/G PLUS-agarose (SC-2003, Santa Cruz Biotechnology) and 8 µl of IP buffer (50 mM Tris-HCl pH 7.5, 150 mM NaCl, 0.5% NP-40, 1 mM EDTA, 3 mM DTT, 1 mM PMSF, 5 µg ml^{-1} leupeptin, 1 µg ml^{-1} aprotinin, 1 µg ml^{-1} pepstatin) overnight at 4 °C with gentle agitation. Frozen tobacco leaves were ground in liquid nitrogen and 500 µl of ground tissue were mixed with 500 µl of IP buffer. These samples were vortexed for 2–3 min and centrifuged at 18,400*g* for 10 min at 4 °C. Supernatant was added to the anti-GFP matrix agarose and the mixture was incubated for 2 h at 4 °C with gentle agitation, followed by centrifugation at 845*g* at 4 °C for 3 min to collect immune complexes. Pellets were washed three times with ice-cold IP buffer, once with 1× PBS buffer and eluted with 50 µl of 2× SDS–PAGE sample buffer. Immunoblotting was performed as previously described[11]. The following antibodies were used to detect the fusion proteins: rabbit anti-GFP (Abcam; ab6556), rat anti-HA (Sigma, 11867423001), anti-rabbit IgG peroxidase-conjugated (SeraCare/KPL; 5220-0283/04-15-06) and anti-rat IgG peroxidase-conjugated (SeraCare/KPL; 5220-0364/04-16-06). All antibodies were diluted 1:2,000 in TBS-T buffer (1× TBS, 0.1% Tween 20) supplemented with 4% non-fat milk. After the final washes, the membranes were processed with SuperSignal West Pico PLUS Chemiluminescent Substrate (Thermo Scientific, 34577) and imaged with a MyECL imager (Thermo Scientific).

Split-luciferase assay. The coding sequences of INP1 and INP2 from *Arabidopsis* and tomato were PCR amplified, cloned into pDONR207 (Invitrogen) and transferred into pCAMBIA1300-^{GW}NLuc and pCAMBIA1300-^{GW}CLuc (ref. [41]) (a gift from D. Mackey, OSU) using the Gateway technology. Resulting constructs were transformed individually into *A. tumefaciens* strain GV3101. Agrobacteria were collected and resuspended in infiltration buffer (10 mM $MgCl_2$, 10 mM MES, 150 µM acetosyringone) at a final concentration of $OD_{600} = 0.8$. Pairwise combinations of suspensions were infiltrated into young tobacco leaves, which were then allowed to grow for 3 d in light. A total 12–16 leaves were collected from five to ten plants, the abaxial side of leaves was sprayed with 1 mM luciferin (Biosynth, L-8220) and kept in the dark at 4 °C for 30 min. The bioluminescence images were captured using Azure Sapphire Biomolecule Imager (Azure Biosystems) and converted to heatmaps using the 16-colour look-up table from ImageJ v.1.53a.

Reporting Summary. Further information on research design is available in the Nature Research Reporting Summary linked to this article.

Data availability

All data supporting the findings of this study are available within the article, Supplementary Information files or from the corresponding author on reasonable request. Source data are provided with this paper.

Received: 5 January 2021; Accepted: 25 May 2021;
Published online: 28 June 2021

References

1. Furness, C. A. & Rudall, P. J. Pollen aperture evolution—a crucial factor for eudicot success? *Trends Plant Sci.* **9**, 154–158 (2004).
2. Zhou, Y. & Dobritsa, A. A. Formation of aperture sites on the pollen surface as a model for development of distinct cellular domains. *Plant Sci.* **288**, 110222 (2019).
3. Heslop-Harrison, J. An interpretation of the hydrodynamics of pollen. *Am. J. Bot.* **66**, 737–743 (1979).
4. Katifori, E., Alben, S., Cerda, E., Nelson, D. R. & Dumais, J. Foldable structures and the natural design of pollen grains. *Proc. Natl Acad. Sci. USA* **107**, 7635–7639 (2010).
5. Vieira, A. M. & Feijó, J. A. Hydrogel control of water uptake by pectins during in vitro pollen hydration of *Eucalyptus globulus*. *Am. J. Bot.* **103**, 437–451 (2016).
6. Zhang, X. et al. Rice pollen aperture formation is regulated by the interplay between OsINP1 and OsDAF1. *Nat. Plants* **6**, 394–403 (2020).
7. Wodehouse, R. P. *Pollen Grains: Their Structure, Identification and Significance in Science and Medicine* (McGraw-Hill, 1935).
8. *PalDat—A Palynological Database* (PalDat, accessed 30 April 2018); www.paldat.org
9. Dobritsa, A. A. & Coerper, D. The novel plant protein INAPERTURATE POLLEN1 marks distinct cellular domains and controls formation of apertures in the *Arabidopsis* pollen exine. *Plant Cell* **24**, 4452–4464 (2012).
10. Dobritsa, A. A., Kirkpatrick, A. B., Reeder, S. H., Li, P. & Owen, H. A. Pollen aperture factor INP1 acts late in aperture formation by excluding specific membrane domains from exine deposition. *Plant Physiol.* **176**, 326–339 (2018).
11. Lee, B. H. et al. *Arabidopsis* protein kinase D6PKL3 is involved in formation of distinct plasma-membrane aperture domains on the pollen surface. *Plant Cell* **30**, 2038–2056 (2018).
12. Li, P. et al. INP1 involvement in pollen aperture formation is evolutionarily conserved and may require species-specific partners. *J. Exp. Bot.* **69**, 983–996 (2018).
13. Dobritsa, A. A. et al. A large-scale genetic screen in *Arabidopsis* to identify genes involved in pollen exine production. *Plant Physiol.* **157**, 947–970 (2011).
14. Reeder, S. H., Lee, B. H., Fox, R. & Dobritsa, A. A. A ploidy-sensitive mechanism regulates aperture formation on the *Arabidopsis* pollen surface and guides localization of the aperture factor INP1. *PLoS Genet.* **12**, e1006060 (2016).
15. Klepikova, A. V., Kasianov, A. S., Gerasimov, E. S., Logacheva, M. D. & Penin, A. A. A high resolution map of the *Arabidopsis thaliana* developmental transcriptome based on RNA-seq profiling. *Plant J.* **88**, 1058–1070 (2016).
16. Sall, K. et al. DELAY OF GERMINATION 1-LIKE 4 acts as an inducer of seed reserve accumulation. *Plant J.* **100**, 7–19 (2019).
17. Kelley, L. A., Mezulis, S., Yates, C. M., Wass, M. N. & Sternberg, M. J. E. The Phyre2 web portal for protein modeling, prediction and analysis. *Nat. Protoc.* **10**, 845–858 (2015).
18. Magnani, E. et al. A comprehensive analysis of microProteins reveals their potentially widespread mechanism of transcriptional regulation. *Plant Physiol.* **165**, 149–159 (2014).
19. Amborella Genome Project. The *Amborella* genome and the evolution of flowering plants. *Science* **342**, 1241089 (2013).
20. Kellogg, E. A. Evolutionary history of the grasses. *Plant Physiol.* **125**, 1198–1205 (2001).
21. Plourde, S. M., Amom, P., Tan, M., Dawes, A. T. & Dobritsa, A. A. Changes in morphogen kinetics and pollen grain size are potential mechanisms of aberrant pollen aperture patterning in previously observed and novel mutants of *Arabidopsis thaliana*. *PLoS Comput. Biol.* **15**, e1006800 (2019).
22. Lukowitz, W., Gillmor, C. S. & Scheible, W.-R. Positional cloning in *Arabidopsis*. Why it feels good to have a genome initiative working for you. *Plant Physiol.* **123**, 795–806 (2000).
23. 1001 Genomes Consortium. 1,135 genomes reveal the global pattern of polymorphism in *Arabidopsis thaliana*. *Cell* **166**, 481–491 (2016).
24. Hou, X. et al. A platform of high-density INDEL/CAPS markers for map-based cloning in *Arabidopsis*. *Plant J.* **63**, 880–888 (2010).
25. Wickett, N. J. et al. Phylotranscriptomic analysis of the origin and early diversification of land plants. *Proc. Natl Acad. Sci. USA* **111**, E4859–E4868 (2014).
26. Van Bel, M. et al. PLAZA 4.0: an integrative resource for functional, evolutionary and comparative plant genomics. *Nucleic Acids Res.* **46**, D1190–D1196 (2018).
27. Capella-Gutiérrez, S., Silla-Martínez, J. M. & Gabaldón, T. trimAl: a tool for automated alignment trimming in large-scale phylogenetic analyses. *Bioinformatics* **25**, 1972–1973 (2009).
28. Kalyaanamoorthy, S., Minh, B. Q., Wong, T. K. F., von Haeseler, A. & Jermiin, L. S. ModelFinder: fast model selection for accurate phylogenetic estimates. *Nat. Methods* **14**, 587–589 (2017).
29. Trifinopoulos, J., Nguyen, L.-T., von Haeseler, A. & Minh, B. Q. W-IQ-TREE: a fast online phylogenetic tool for maximum likelihood analysis. *Nucleic Acids Res.* **44**, W232–W235 (2016).
30. Minh, B. Q. et al. IQ-TREE 2: new models and efficient methods for phylogenetic inference in the genomic era. *Mol. Biol. Evol.* **37**, 1530–1534 (2020).
31. Letunic, I. & Bork, P. Interactive tree of life (iTOL) v4: recent updates and new developments. *Nucleic Acids Res.* **47**, W256–W259 (2019).
32. Xie, K., Zhang, J. & Yang, Y. Genome-wide prediction of highly specific guide RNA spacers for CRISPR-Cas9-mediated genome editing in model plants and major crops. *Mol. Plant* **7**, 923–926 (2014).
33. Wang, Z.-P. et al. Egg cell-specific promoter-controlled CRISPR/Cas9 efficiently generates homozygous mutants for multiple target genes in *Arabidopsis* in a single generation. *Genome Biol.* **16**, 144 (2015).
34. Xing, H.-L. et al. A CRISPR/Cas9 toolkit for multiplex genome editing in plants. *BMC Plant Biol.* **14**, 327 (2014).
35. Clough, S. J. & Bent, A. F. Floral dip: a simplified method for *Agrobacterium*-mediated transformation of *Arabidopsis thaliana*. *Plant J.* **16**, 735–743 (1998).
36. Dobritsa, A. A. et al. LAP5 and LAP6 encode anther-specific proteins with similarity to chalcone synthase essential for pollen exine development in *Arabidopsis thaliana*. *Plant Physiol.* **153**, 937–955 (2010).
37. García-Nafría, J., Watson, J. F. & Greger, I. H. IVA cloning: a single-tube universal cloning system exploiting bacterial In Vivo Assembly. *Sci. Rep.* **6**, 27459 (2016).
38. Wang, L., Kim, J. & Somers, D. E. Transcriptional corepressor TOPLESS complexes with pseudoresponse regulator proteins and histone deacetylases to regulate circadian transcription. *Proc. Natl Acad. Sci. USA* **110**, 761–766 (2013).
39. Voinnet, O., Pinto, Y. M. & Baulcombe, D. C. Suppression of gene silencing: a general strategy used by diverse DNA and RNA viruses of plants. *Proc. Natl Acad. Sci. USA* **96**, 14147–14152 (1999).
40. Kim, J., Geng, R., Gallenstein, R. A. & Somers, D. E. The F-box protein ZEITLUPE controls stability and nucleocytoplasmic partitioning of GIGANTEA. *Development* **140**, 4060–4069 (2013).
41. Shen, M. et al. HOS15 is a transcriptional corepressor of NPR1-mediated gene activation of plant immunity. *Proc. Natl Acad. Sci. USA* **117**, 30805–30815 (2020).

Acknowledgements

Funding for this project was provided to A.A.D. by the US National Science Foundation (MCB-1817835). We acknowledge the support from the US National Institutes of Health grant no. R35GM131760 (to I.B.Z.), the TRONDBUSS program (OSU and Norwegian Science and Technology University) (to I. M.M.), Herta Camerer Gross Postdoctoral Research Fellowship (to R.W.), University graduate fellowships (to P.C. and K.A.), OSU Mayers Undergraduate Summer Research Scholarship (to P.A.), NSF-REU supplement mechanism (to P.A. and A.H.), iCAPS internship from the Center for Applied Science (to A.H.), Undergraduate Research Scholarship from the OSU Arts and Sciences Honors Committee (to A.H.) and a Dr. Elizabeth Wagner Scholarship from the Department of Molecular Genetics at OSU (to A.H.). We thank members of the Dobritsa laboratory for discussions, Y. Zhou for help with phylogenetic analysis, V. Edwards, N. Weyrick and S. Knapp for technical help, D. Somers and D. Mackey for vectors, Arabidopsis Biological Resource Center for DNA stocks and the NCI-subsidized Genomics Facility at the OSU Comprehensive Cancer Center (CCSG:P30CA016058) for sequencing.

Author contributions

B.H.L., R.W. and A.A.D. conceived and designed the experiments. B.H.L., R.W., I.M.M., S.H.R., P.A., M.H.T., K.A., P.C., A.H. and A.A.D. performed the experiments. E.P.A., A.A.D. and I.B.Z. performed phylogenetic analysis. B.H.L., R.W., I.M.M., K.A., P.C., E.P.A. and A.A.D. analysed the data. A.A.D. wrote the article and all authors revised and approved the final manuscript.

Competing interests

The authors declare no competing interests.

Additional information

Extended data is available for this paper at https://doi.org/10.1038/s41477-021-00951-9.

Supplementary information The online version contains supplementary material available at https://doi.org/10.1038/s41477-021-00951-9.

Correspondence and requests for materials should be addressed to A.A.D.

Peer review information *Nature Plants* thanks Sheila McCormick, Dabing Zhang and the other, anonymous, reviewer(s) for their contribution to the peer review of this work.

Reprints and permissions information is available at www.nature.com/reprints.

Publisher's note Springer Nature remains neutral with regard to jurisdictional claims in published maps and institutional affiliations.

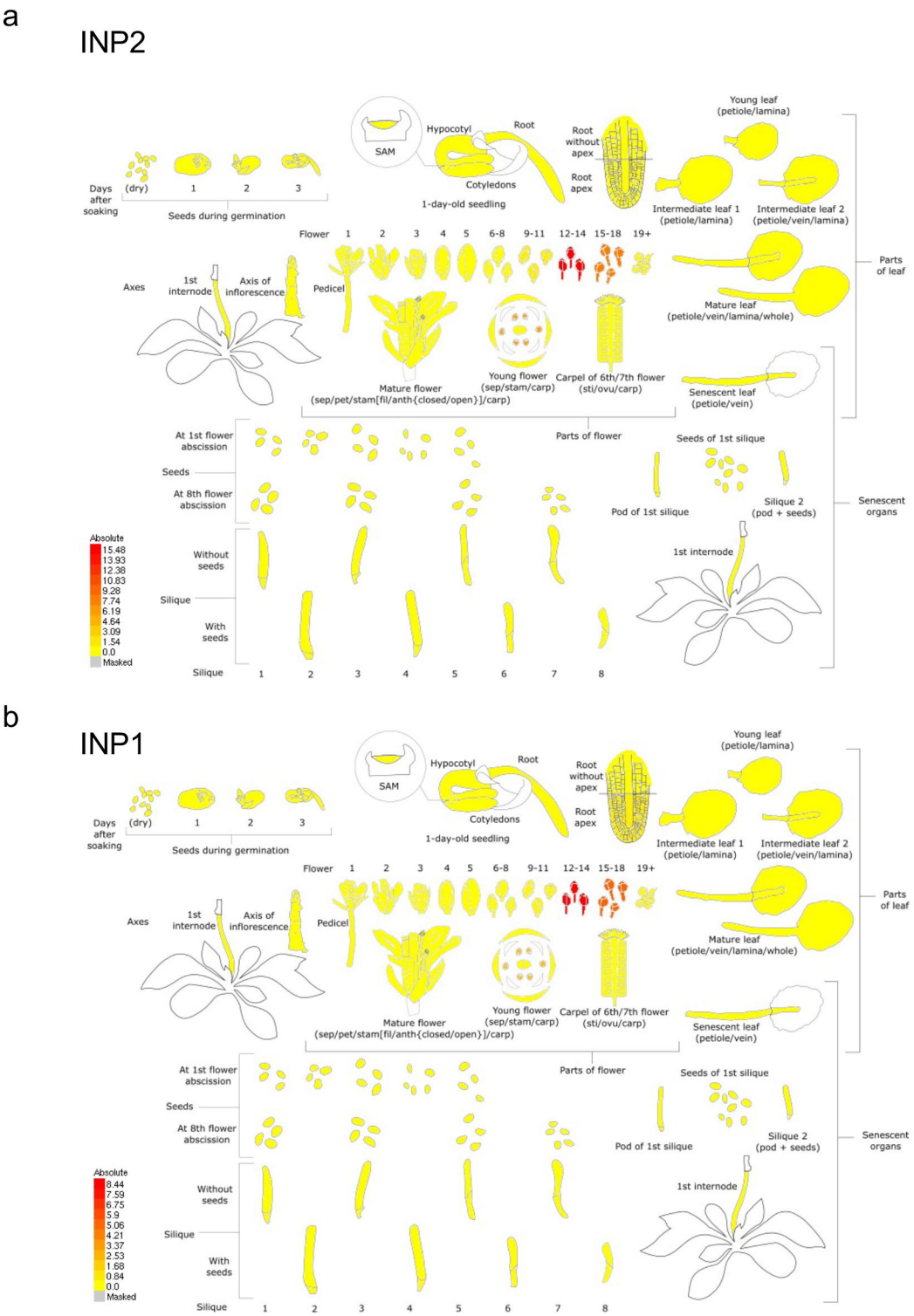

Extended Data Fig. 1 | *INP2* and *INP1* display similar expression patterns, with both genes showing highest expression in young developing buds. The RNA-seq data for INP2 (**a**) and INP1 (**b**) are from the dataset of Klepikova et al.[15] and visualized with the BAR eFP Browser.

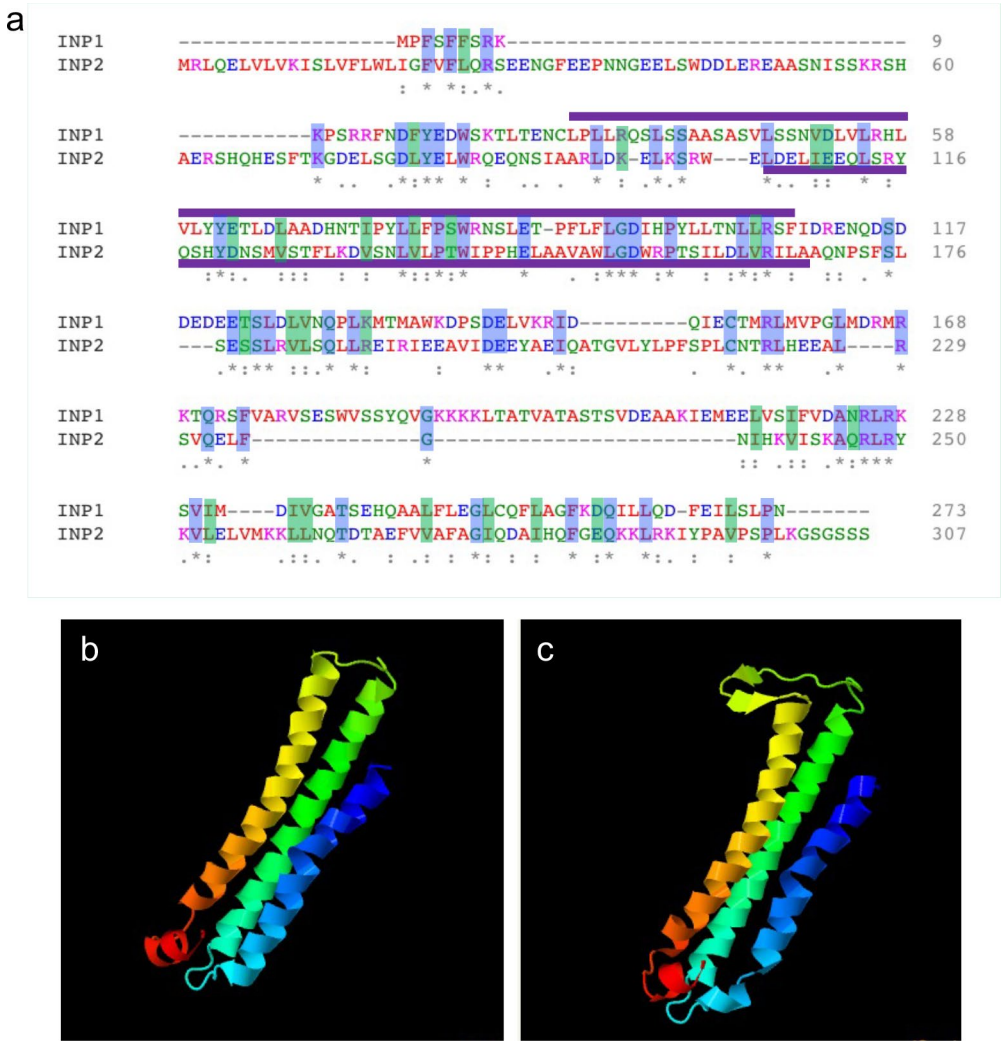

Extended Data Fig. 2 | INP1 and INP2 proteins both contain the DOG1 domain and have similar structural organization predicted for their C-terminal parts. a, Protein alignment between INP1 and INP2 proteins. Identical and similar (V/I/L, D/E, K/R, N/Q and S/T) residues are shaded, respectively, in blue and green. The positions of the DOG1 domains predicted by Pfam are indicated by purple lines. **b-c**, Protein structures predicted by Phyre2 for C-terminal parts of INP1 (**b**) and INP2 (**c**) (confidence: >97% for both proteins). In both cases, the modelled regions cover 114 amino acids, which constitute, respectively, 42% of INP1 and 37% of INP2. The same template (c4clvB, nickel-cobalt-cadmium resistance protein NccX from *Cupriavidus metallidurans 31a*) was selected by the program in both cases.

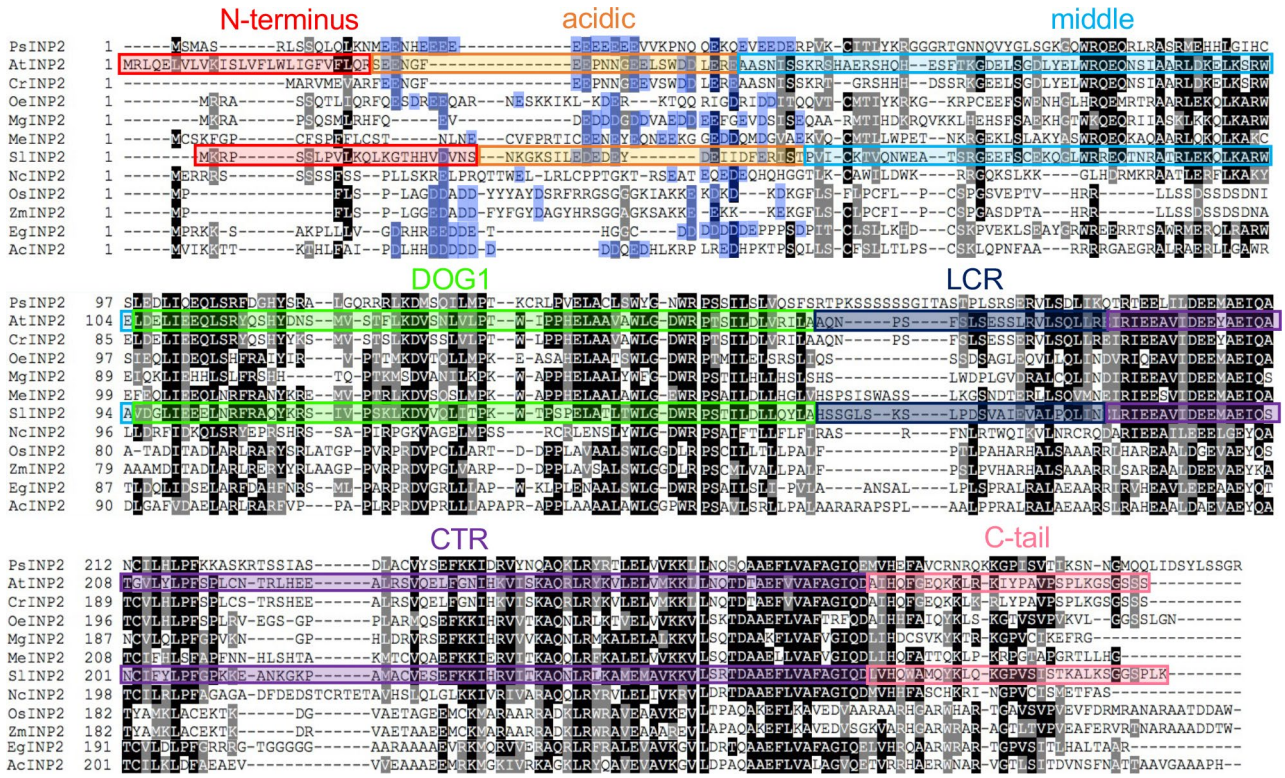

Extended Data Fig. 3 | Alignment of INP2 proteins from representatives of different angiosperm taxa. The following species were used (from top to bottom): *Papaver somniferum* (basal eudicots, Papaveraceae), *Arabidopsis thaliana* (rosids, Brassicaceae) *Capsella rubella* (rosids, Brassicaceae), *Olea europea* (asterids, Oleaceae), *Mimulus guttatus* (asterids, Phrymacae), *Manihot esculenta* (rosids, Euphorbiaceae), *Solanum lycopersicum* (asterids, Solanaceae), *Nymphaea colorata* (basal angiosperms, ANA, Nympheaceae), *Oryza sativa* (monocots, Poaceae), *Zea mays* (monocots, Poaceae), *Elaeis guineensis* (monocots, Arecaceae), *Ananas comosus* (monocots, Bromeliaceae). The seven regions selected for creating AtINP2/SlINP2 chimeras are indicated by differently coloured rectangles. Aspartate (D) and glutamate (E) residues in the acidic region are shaded in blue. Black shading indicates identical amino acids and grey shading indicates similar amino acids present at the same position in at least half of the aligned proteins.

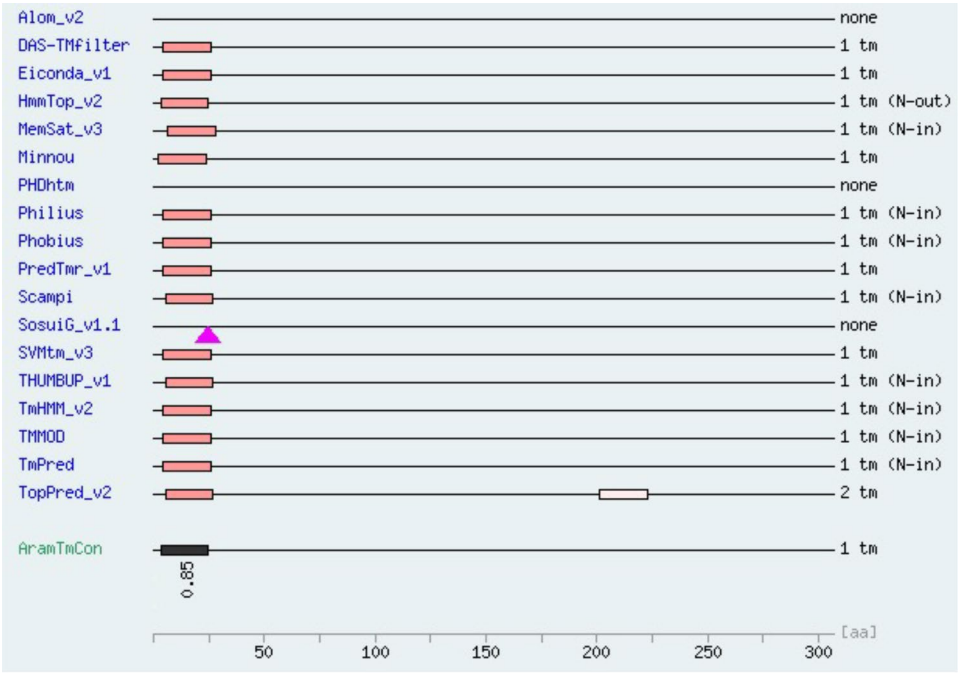

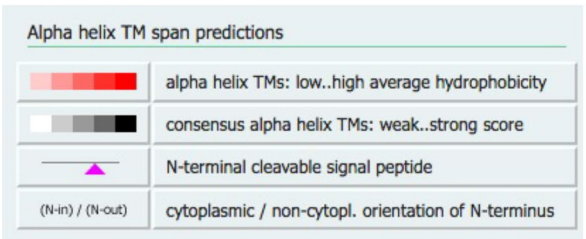

Extended Data Fig. 4 | Arabidopsis INP2 likely contains a transmembrane domain at its N terminus. Multiple TM discovery algorithms predict existence of the transmembrane domain at the N terminus of INP2 from *Arabidopsis thaliana* (AtINP2), with the consensus score of 0.85 generated by the plant membrane protein database Aramemnon (AramTMCon).

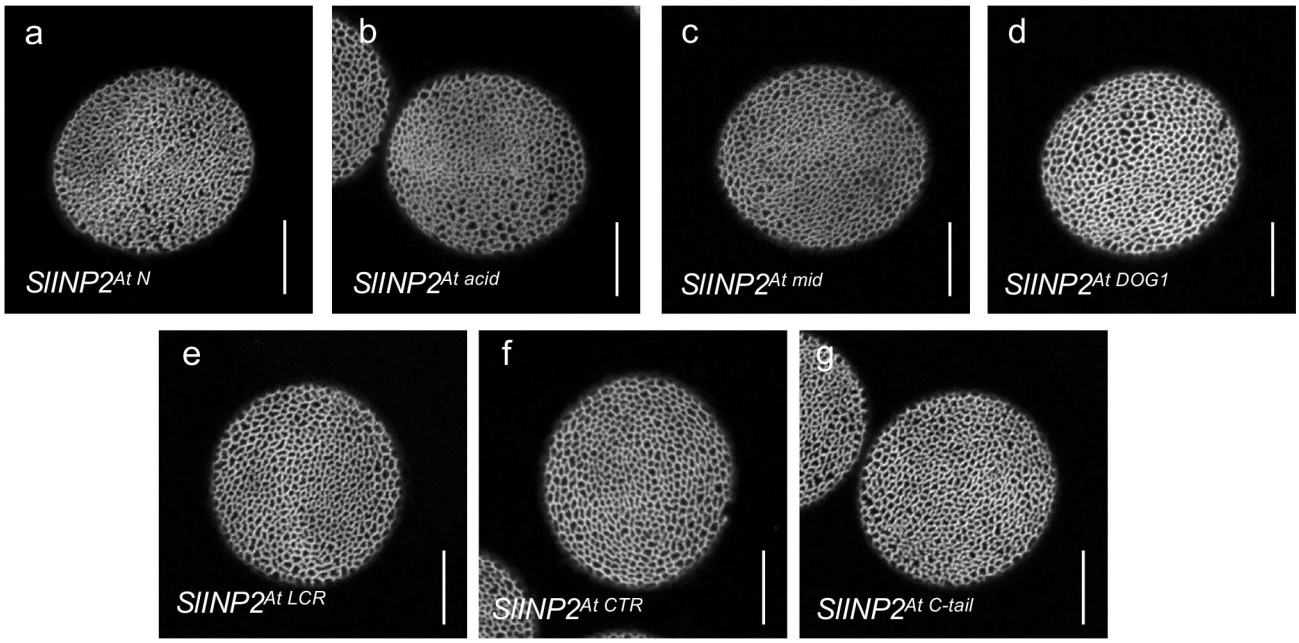

Extended Data Fig. 5 | None of the seven AtINP2 regions is sufficient on its own to convert SlINP2 into a protein able to function in Arabidopsis. Confocal images of pollen grains produced by the transgenic *inp2* plants expressing seven versions of chimeric *SlINP2* constructs in which one region at a time was replaced with the corresponding regions from *AtINP2*. At least 10 independent T_1 lines were tested for each construct (≥ 50 pollen grains per line), with similar results. Scale bars = 10 µm.

nature research

Corresponding author(s): Anna Dobritsa

Last updated by author(s): May 21, 2021

Reporting Summary

Nature Research wishes to improve the reproducibility of the work that we publish. This form provides structure for consistency and transparency in reporting. For further information on Nature Research policies, see our Editorial Policies and the Editorial Policy Checklist.

Statistics

For all statistical analyses, confirm that the following items are present in the figure legend, table legend, main text, or Methods section.

n/a	Confirmed	
☐	☒	The exact sample size (*n*) for each experimental group/condition, given as a discrete number and unit of measurement
☐	☒	A statement on whether measurements were taken from distinct samples or whether the same sample was measured repeatedly
☒	☐	The statistical test(s) used AND whether they are one- or two-sided *Only common tests should be described solely by name; describe more complex techniques in the Methods section.*
☒	☐	A description of all covariates tested
☒	☐	A description of any assumptions or corrections, such as tests of normality and adjustment for multiple comparisons
☒	☐	A full description of the statistical parameters including central tendency (e.g. means) or other basic estimates (e.g. regression coefficient) AND variation (e.g. standard deviation) or associated estimates of uncertainty (e.g. confidence intervals)
☒	☐	For null hypothesis testing, the test statistic (e.g. *F*, *t*, *r*) with confidence intervals, effect sizes, degrees of freedom and *P* value noted *Give P values as exact values whenever suitable.*
☒	☐	For Bayesian analysis, information on the choice of priors and Markov chain Monte Carlo settings
☒	☐	For hierarchical and complex designs, identification of the appropriate level for tests and full reporting of outcomes
☒	☐	Estimates of effect sizes (e.g. Cohen's *d*, Pearson's *r*), indicating how they were calculated

Our web collection on statistics for biologists contains articles on many of the points above.

Software and code

Policy information about availability of computer code

Data collection	For bioinformatics analysis, BLAST search was conducted using NCBI website (http://www.ncbi.nlm.nih.gov/), Phytozome v. 12.1 (https://phytozome.jgi.doe.gov/pz/portal.html), the 1,000 Plants project (OneKP-China National Gene Bank (https://db.cngb.org/onekp/)24 and PLAZA (https://bioinformatics.psb.ugent.be/plaza/). For confocal imaging, NIS Elements v.4.20 software (Nikon) was used.
Data analysis	3D reconstruction of tetrads was done using NIS Elements v.4.20 software (Nikon). For multiple sequences alignment, MAFFT v7.017 (L-INS-i algorithm) was used (https://www.ebi.ac.uk/Tools/msa/mafft/). The IQ-TREE program v. 1.6.12, (http://www.iqtree.org/) was used to construct phylogenetic trees. The phylogenetic trees were visualized in iTOL v. 5 (https://itol.embl.de/). Split-luciferase assay analysis was done with ImageJ v. 1.53a.

For manuscripts utilizing custom algorithms or software that are central to the research but not yet described in published literature, software must be made available to editors and reviewers. We strongly encourage code deposition in a community repository (e.g. GitHub). See the Nature Research guidelines for submitting code & software for further information.

Data

Policy information about availability of data

All manuscripts must include a data availability statement. This statement should provide the following information, where applicable:

- Accession codes, unique identifiers, or web links for publicly available datasets
- A list of figures that have associated raw data
- A description of any restrictions on data availability

Public RNA-seq data for gene expression analysis ,were obtained from the TRAVA database (travadb.org).
Protein sequences were obtained from TAIR (https://www.arabidopsis.org/), NCBI (http://www.ncbi.nlm.nih.gov/), Phytozome v. 12.1 (https://phytozome.jgi.doe.gov/pz/portal.html), the 1,000 Plants project (OneKP-China National Gene Bank (https://db.cngb.org/onekp/)24 and PLAZA (https://

bioinformatics.psb.ugent.be/plaza/).
Markers for mapping were generated using the 1,001 Genomes Project database (http://signal.salk.edu/atg1001/index.php)23 and the Arabidopsis Mapping Platform (http://amp.genomics.org.cn/).
Fig. 4C contains associated Source data.
All data supporting the findings of this study are available within the article, Supplementary Information files or from the corresponding author upon reasonable request.

Field-specific reporting

Please select the one below that is the best fit for your research. If you are not sure, read the appropriate sections before making your selection.

☒ Life sciences ☐ Behavioural & social sciences ☐ Ecological, evolutionary & environmental sciences

For a reference copy of the document with all sections, see nature.com/documents/nr-reporting-summary-flat.pdf

Life sciences study design

All studies must disclose on these points even when the disclosure is negative.

Sample size	Sample sizes were consistent with those in our and others' previously published similar studies (e.g. Lee et al. (2018) Plant Cell 30:2038-2056; Zhang et al. (2020) Nat. Plants 6, 394–403). All experiments were performed using at least three independent biological replicates. For transgenic lines, a minimum of eight independent lines were created and analyzed. Sample sizes and the number of times an experiment was performed are described in figure legends and main text.
Data exclusions	No data were excluded.
Replication	At least three independent biological replicates were used for each experiment, with similar results. For transgenic lines, a minimum of eight independent lines were created and analyzed, with similar results.
Randomization	Plants of different genotypes were used as study groups. When more plants were available than the required sample size, plants were chosen randomly for analysis.
Blinding	Experiments were not blinded. Data were collected according to the genotypes of samples. Since comparisons were generally qualitative, blinding was not relevant.

Reporting for specific materials, systems and methods

We require information from authors about some types of materials, experimental systems and methods used in many studies. Here, indicate whether each material, system or method listed is relevant to your study. If you are not sure if a list item applies to your research, read the appropriate section before selecting a response.

Materials & experimental systems

n/a	Involved in the study
☐	☒ Antibodies
☒	☐ Eukaryotic cell lines
☒	☐ Palaeontology and archaeology
☒	☐ Animals and other organisms
☒	☐ Human research participants
☒	☐ Clinical data
☒	☐ Dual use research of concern

Methods

n/a	Involved in the study
☒	☐ ChIP-seq
☒	☐ Flow cytometry
☒	☐ MRI-based neuroimaging

Antibodies

Antibodies used	For immunoprecipitation: anti-GFP antibody (monoclonal (clone 3E6, lot 1711553), mouse, Molecular Probes by ThermoFisher Scientific, #A-11120). To detect proteins on Westerns (all antibodies were used at 1:2000 dilution): anti-GFP antibody (polyclonal, rabbit, Abcam; ab6556) anti-HA antibody (monoclonal (clone 3F10), rat, Sigma, 11867423001) anti-rabbit IgG peroxidase-conjugated antibodies (SeraCare/KPL; 5220-0283/04-15-06) anti-rat IgG peroxidase-conjugated antibodies (SeraCare/KPL; 5220-0364/04-16-06)
Validation	Anti-GFP monoclonal: https://www.thermofisher.com/antibody/product/GFP-Antibody-clone-3E6-Monoclonal/A-11120 and publications listed thereof. Anti-GFP polyclonal: https://www.abcam.com/gfp-antibody-ab6556.html and publications listed thereof. Anti-HA: https://www.sigmaaldrich.com/content/dam/sigma-aldrich/docs/Roche/Bulletin/1/roahahabul.pdf

Anti-rabbit IG peroxidase-conjugated: https://www.seracare.com/AntiRabbit-IgG-HL-Antibody-PeroxidaseLabeled-5220-0283/
Anti-rat IG peroxidase-conjugated: https://www.seracare.com/search/?q=5220-0364&searchType=product

nature portfolio

https://doi.org/10.1038/s41477-021-00951-9

Supplementary information

A species-specific functional module controls formation of pollen apertures

In the format provided by the authors and unedited

Supplementary Table 1. Amino acid sequence identity between AtINP1, AtINP2 and their respective orthologs from a variety of angiosperm taxa.

Species	Clade	Sub Clade	Sub clade	Order	Family	INP1	INP2	INP1: Identity to AtINP1	INP2: Identitity to AtINP2
Arabidopsis thaliana	Eudicots	Eurosids	Malvids	Brassicales	Brassicaceae	At4g22600	At1g15320	100%	100%
Arabidopsis lyrata	Eudicots	Eurosids	Malvids	Brassicales	Brassicaceae	XM_002867712	XM_002892814	94%	90%
Capsella rubella	Eudicots	Eurosids	Malvids	Brassicales	Brassicaceae	XM_006285378	XM_006303615	92%	90%
Eutrema salsugineum	Eudicots	Eurosids	Malvids	Brassicales	Brassicaceae	XM_006413577	XP_006416922	84%	82%
Tarenaya hassleriana	Eudicots	Eurosids	Malvids	Brassicales	Cleomaceae	XP_010539222	XP_010538005	70%	70%
Carica papaya	Eudicots	Eurosids	Malvids	Brassicales	Caricaceae	XM_022046188	XM_022042844	56%	44%
Theobroma cacao	Eudicots	Eurosids	Malvids	Malvales	Malvaceae	XP_007039914	XP_007023253	54%	47%
Gossipium raimondii	Eudicots	Eurosids	Malvids	Malvales	Malvaceae	XP_012471971	XP_012442564	50%	49%
Herrania umbratica	Eudicots	Eurosids	Malvids	Malvales	Malvaceae	XM_021435636	XM_021442724	55%	48%
Manihot esculenta	Eudicots	Eurosids	Fabids	Malpighiales	Euphorbiaceae	XP_021631264	Manes.04G112100	54%	45%
Ricinus communis	Eudicots	Eurosids	Fabids	Malpighiales	Euphorbiaceae	XP_002529792	XP_002517657	53%	45%
Hevea brasiliensis	Eudicots	Eurosids	Fabids	Malpighiales	Euphorbiaceae	XM_021805081	XM_021780609	55%	44%
Populus trichocarpa	Eudicots	Eurosids	Fabids	Malpighiales	Salicaceae	XM_024587580	XP_006369313	52%	52%
Linum usitatissimum	Eudicots	Eurosids	Fabids	Malpighiales	Linaceae	Lus10028923 (Phytozome)	Lus10025746 (Phytozome)	49%	38%
Citrus cinensis	Eudicots	Eurosids	Fabids	Sapindales	Rutaceae	XM_015529742	XP_015386244	50%	48%
Pistacia vera	Eudicots	Eurosids	Fabids	Sapindales	Anacardiaceae	XM_031405325	XM_031431563	50%	48%
Fragaria vesca	Eudicots	Eurosids	Fabids	Rosales	Rosaceae	XM_004300662	XP_004305502	47%	47%
Prunus persica	Eudicots	Eurosids	Fabids	Rosales	Rosaceae	XM_007210501	XP_020416177	49%	47%
Ziziphus jujuba	Eudicots	Eurosids	Fabids	Rosales	Rhamnaceae	XM_016045621	XP_015870799	49%	47%
Cannabis sativa	Eudicots	Eurosids	Fabids	Rosales	Cannabaceae	XM_030645895	XM_030632112	51%	48%
Quercus suber	Eudicots	Eurosids	Fabids	Fagales	Fagaceae	XM_024052895	XM_024036728	50%	45%
Juglans regia	Eudicots	Eurosids	Fabids	Fagales	Juglandaceae	XM_018992647	XP_018851749	50%	47%
Vitis vinifera	Eudicots	Rosids		Vitales	Vitaceae	XM_010648242	XP_010654806	46%	45%
Solanum lycopersicum	Eudicots	Euasterids	Lamiids	Solanales	Solanaceae	XM_004245692	XP_004236461	46%	43%
Ipomaea nil	Eudicots	Euasterids	Lamiids	Solanales	Convolvulaceae	XM_019340312	XP_019159957	48%	42%
Mimulus guttatus	Eudicots	Euasterids	Lamiids	Lamiales	Phrymaceae	XM_012990426	XP_012856236	45%	41%
Olea europea	Eudicots	Euasterids	Lamiids	Lamiales	Oleaceae	XM_023026469	XM_022994362	45%	43%
Sesamum indicum	Eudicots	Euasterids	Lamiids	Lamiales	Pedaliaceae	XM_011083080	XM_020692503	47%	45%
Coffea arabica	Eudicots	Euasterids	Lamiids	Gentianales	Rubiaceae	XM_027226234	XM_027270435	46%	42%
Lactuca sativa	Eudicots	Euasterids	Campanulid	Asterales	Asteraceae	XP_023753693	XM_023894801	45%	37%
Helianthus annuus	Eudicots	Euasterids	Campanulid	Asterales	Asteraceae	XM_022149160	XM_022162388	44%	37%
Daucus carota	Eudicots	Euasterids	Campanulid	Apiales	Apiaceae	XM_017377544	XM_017362523	44%	41%
Camellia sinensis	Eudicots	Asterids		Ericales	Theacaceae	XM_028205791	XM_028195317	49%	48%
Spinacia oleracea	Eudicots	Core eudicots/Superast		Caryophylalles	Amaranthaceae	XM_022000275	XM_022007145	41%	42%
Nelumbo nucifera	Basal eudicots			Proteales	Nelumbonaceae	XP_010259014	XP_010241626	46%	46%
Papaver somniferum	Basal eudicots			Ranunculales	Papaveraceae	XM_026602809	XM_026587879	40%	36%
Aquilegia coerulea	Basal eudicots			Ranunculales	Ranunculaceae	Aqcoe7G079000 (Phytozome)	Aqcoe7G382900 (Phytozome)	46%	42%
Elaeis guineensis	Monocots	Commelinids		Arecales	Arecaceae	XM_010921594	XP_010928340	44%	34%
Phoenix dactilifera	Monocots	Commelinids		Arecales	Arecaceae	XM_008788847	XM_026804442	44%	34%
Ananas comosus	Monocots	Commelinids		Poales	Bromeliaceae	Aco011729, Phytozome	XM_020246879	39%	25%
Oryza sativa	Monocots	Commelinids		Poales	Poaceae	XP_025878546	XM_015755361	35%	21%
Brachypodium distachyon	Monocots	Commelinids		Poales	Poaceae	XM_024460675	XP_003576910	35%	20%
Zea mays	Monocots	Commelinids		Poales	Poaceae	NP_001130869	XP_008649809	36%	21%
Setaria italica	Monocots	Commelinids		Poales	Poaceae	XM_004953314	XP_004956307	35%	21%
Sorgum bicolor	Monocots	Commelinids		Poales	Poaceae	XM_002452752	XP_002441305	36%	21%
Laurelia sempervirens	Magnoliids			Laurales	Atherospermataceae	gnl|onekp|WAIL_scaffold_2020264	gnl|onekp|WAIL_scaffold_2068545	46%	48%
Austrobaileya scandens	Basal angiosperm	ANA		Austrobaileyales	Austrobaileyaceae	gnl|onekp|FZJL_scaffold_2015050	?	46%	N/A
Nymphaea colorata	Basal angiosperm	ANA		Nymphaeales	Nymphaeaceae	XM_031628012	XM_031628356	40%	31%
Amborella trichopoda	Basal angiosperm	ANA		Amborellales	Amborellaceae	No	No	N/A	N/A

Color coding according to order/clade is the same as in Fig. 5

Supplementary Table 2. Primers used in this study.

Construct/Purpose	Primer name (restriction enzyme)	Sequence (5' to 3'; restriction enzyme recognition sites are underlined)
INP2pr:INP2 ORF (*INP2* promoter and *INP2* ORF fragments)	INP2pr-IF-F (*Sac*I)	ACAAAAGCTGGAGCTCGCTGTGATCTTCTTTGCTCTTC
	INP2pr-IF-R (*Bam*HI)	GGATCCTGCACACTCAAATCCTAAAATGC
	INP2-ORF-IF-F (*Bam*HI)	GAGTGTGCAGGATCCATGAGATTACAAGAGTTGGTTC
	INP2-stop-SpeI-R (*Spe*I)	GGAAACTAGTTCAACTAGATGATCCTGATCC
INP2pr:gINP2 (Fragment composed of INP2 genic + ~0.5kb downstream regions)	INP2-ORF-IF-F (*Bam*HI)	GAGTGTGCAGGATCCATGAGATTACAAGAGTTGGTTC
	gINP2-SpeI-R (*Spe*I)	GGAAACTAGTTGCTGTATGGCGCGGGTTATC
INP2pr:H2B-RFP (H2B-RFP fragment)	H2BRFPinfAF (AgeI)	ATCCCCGGGTACCGGTGAATTCATGGCGAAGGCAGATAAGAAACC
	H2BRFPinfAR (*Spe*I)	AGCGTACCGGACTAGTTTAGGCGCCGGTGGAGTGGCGGC
INP2pr:gSlINP2 (SlINP2 genomic fragment)	BamHI-SlINP2-BF (*Bam*HI)	GGAAGGATCCATGAAGCGGCCTTCTTCTCTG
	SpeI-SlINP2-AR (*Spe*I)	GGAAACTAGTCTTTTCTAAAGCCGAACGGTAAAC
Genotyping for SlINP1 transgene	2-Sl-F	GGCGACTCAGAATCCGAAATTGAC
	Sly INP1-R-NcoI (*Nco*I)	GGAACCATGGCTAATTCCAAAGAACACTTGTCAAATTGAC
Genotyping for SlINP2 transgene	AD23	TTTGTCTTCCTGCAACGTAACAAAGGAAAATCTATACTCGAAGATGAAGAC
	AD8	CTCTTCGATGCGTATCTCGTTGATCAATTGGGGCAATGCCAC
CAPS marker for inp1-1 (mutant allele cut with SacI)	22600-DF	ccatttagacaagggcttg
	22600-DR	AACTTGATACGACGAGACC
dCAPS marker for inp2-1	At1g15320-BF	GAGAGATCTCACCAACACGAATC

(mutant allele cut with AccI)		
	AD402	CGCAATGCTGTTCTGTTCTTGCGTC
SlINP2 ORF-pGEM-T-Easy (subcloning SlINP2 ORF into pGEM-T-Easy with IVA)	AD19 (*Bam*HI)	CAACGCGTTGGGGGATCCATGAAGCGGCCTTCTTCTCTG
	AD16 (*Spe*I)	CCGGCCGCCATGACTAGTCTACTTAAGTGGGCTACCACCAGAC
	AD17 (*Bam*HI)	GGATCCCCCAACGCGTTGGATGC
	AD14 (*Spe*I)	ACTAGTCATGGCGGCCGGGA
SlINP2 ORF-pGEM-T-Easy (subcloning SlINP2 ORF into pGEM-T-Easy with IVA)	pGEM-INP2-IF-F (*Bam*HI)	ATCCAACGCGTTGGGGGATCCATGAGATTACAAGAGTTGGTTCT
	INP2-pGEM-IF-R (*Spe*I)	CTCCCGGCCGCCATGACTAGTTCAACTAGATGATCCTGATCCCT
1-AtINP2^{SlN}	AD19 (*Bam*HI)	CAACGCGTTGGGGGATCCATGAAGCGGCCTTCTTCTCTG
	AD20	AAATCCATTCTCTTCACTAGAATTGACATCAACGTGATGAGTTCC
	AD17 (*Bam*HI)	GGATCCCCCAACGCGTTGGATGC
	AD18	AGTGAAGAGAATGGATTTGAAGAACCAAAC
2-AtINP2^{Slacid}	AD23	TTTGTCTTCCTGCAACGTAACAAAGGAAAATCTATACTCGAAGATGAAGAC
	AD24	TGATATATTACTAGCAGCTGTGCTGATTCTCTCGAAATCGATGATC
	AD21	ACGTTGCAGGAAGACAAACC
	AD22	GCTGCTAGTAATATATCATCTAAAAGATCTCATGC
3-AtINP2^{Slmid}	AD27	GATGATCTGGAGAGAGAACCTGTAATTTGCAAAACAGTACAAAATTGG
	AD28	TTCAATCAGTTCATCGAGTGCCCATCTTGCTTTTAGCTGTTTCTC
	AD25	TTCTCTCTCCAGATCATCCCAGGAAAG
	AD26	CTCGATGAACTGATTGAAGAACAGCTGAG
4-AtINP2^{SlDOG1}	AD3	CTAAAATCCAGGTGGGAAGTGGATGGACTTATCGAAGAAGAACTC
	AD4	GAAGGAGGGGTTTTGAGCGGCTAAGTATTGAAGAAGATCCAGGATTG
	AD1	TTCCCACCTGGATTTTAGCTCTTTGTC
	AD2	GCTCAAAACCCCTCCTTCTCTC
5-AtINP2^{SlLCR}	AD7	CTTGTCCGCATTCTGGCACATTCATCTGGGCTTTCAAAATCTCTAC
	AD8	CTCTTCGATGCGTATCTCGTTGATCAATTGGGGCAATGCCAC
	AD5	TGCCAGAATGCGGACAAGGTC

	AD6	GAGATACGCATCGAAGAGGCCGTTA
6-AtINP2^{SlCTR}	AD11	CTCTCTCAGCTTTTACGTGAGTTACGAATCGAGG AGGCGGTGA
	AD12	CTGGTGTATGGCGTCTTGAATTCCAGCAAAAGCA ACCAAAAACTC
	AD9	ACGTAAAAGCTGAGAGAGCACG
	AD10	CAAGACGCCATACACCAGTTTGG
7-AtINP2$^{SlC\text{-}tail}$	AD15	GTCGCATTTGCAGGGATTCAAGATTTGGTTCATC AATGGGCTATG
	AD16 (*Spe*I)	CCGGCCGCCATGACTAGTCTACTTAAGTGGGCTA CCACCAGAC
	AD13	AATCCCTGCAAATGCGACCAC
	AD14 (*Spe*I)	ACTAGTCATGGCGGCCGGGA
1-SlINP2^{AtN}	pGEM-INP2-IF-F (*Bam*HI)	ATCCAACGCGTTGGGGGATCCATGAGATTACAAG AGTTGGTTCT
	AD21	ACGTTGCAGGAAGACAAACC
	AD17 (*Bam*HI)	GGATCCCCCAACGCGTTGGATGC
	AD23	TTTGTCTTCCTGCAACGTAACAAAGGAAAATCTAT ACTCGAAGATGAAGAC
2-SlINP2^{Atacid}	AD20	AAATCCATTCTCTTCACTAGAATTGACATCAACGT GATGAGTTCC
	AD27	GATGATCTGGAGAGAGAACCTGTAATTTGCAAAA CAGTACAAAATTGG
	AD18	AGTGAAGAGAATGGATTTGAAGAACCAAAC
	AD25	TTCTCTCTCCAGATCATCCCAGGAAAG
3-SlINP2^{Atmid}	AD24	TGATATATTACTAGCAGCTGTGCTGATTCTCTCGA AATCGATGATC
	AD3	CTAAAATCCAGGTGGGAAGTGGATGGACTTATCG AAGAAGAACTC
	AD22	GCTGCTAGTAATATATCATCTAAAAGATCTCATGC
	AD1	TTCCCACCTGGATTTTAGCTCTTTGTC
4-SlINP2^{AtDOG1}	AD28	TTCAATCAGTTCATCGAGTGCCCATCTTGCTTTTA GCTGTTTCTC
	AD27	GATGATCTGGAGAGAGAACCTGTAATTTGCAAAA CAGTACAAAATTGG
	AD26	CTCGATGAACTGATTGAAGAACAGCTGAG
	AD5	TGCCAGAATGCGGACAAGGTC
5-SlINP2^{AtLCR}	AD2	GCTCAAAACCCCTCCTTCTCTC
	AD9	ACGTAAAAGCTGAGAGAGCACG
	AD4	GAAGGAGGGGTTTTGAGCGGCTAAGTATTGAAGA AGATCCAGGATTG
	AD11	CTCTCTCAGCTTTTACGTGAGTTACGAATCGAGG AGGCGGTGA
6-SlINP2^{AtCTR}	AD8	CTCTTCGATGCGTATCTCGTTGATCAATTGGGGC AATGCCAC

	AD15	GTCGCATTTGCAGGGATTCAAGATTTGGTTCATC AATGGGCTATG
	AD6	GAGATACGCATCGAAGAGGCCGTTA
	AD13	AATCCCTGCAAATGCGACCAC
7-SlINP2$^{AtC\text{-}tail}$	AD12	CTGGTGTATGGCGTCTTGAATTCCAGCAAAAGCA ACCAAAAACTC
	AD14 (*Spe*I)	ACTAGTCATGGCGGCCGGGA
	AD10	CAAGACGCCATACACCAGTTTGG
	INP2-pGEM-IF-R (*Spe*I)	CTCCCGGCCGCCATGACTAGTTCAACTAGATGAT CCTGATCCCT
gRNA sequence for *INP2* CRISPR construct in pHEE401E vector	Oligo-01-F-INP2-T1	ATTGAGACTTGTACGAACTGTGG
	Oligo-R-INP2-T1	AAACCCACAGTTCGTACAAGTCT
35Spr:nYFP-AtINP1	AD17-BHL (*Pac*I)	CCCTTAATTAACATGCCTTTCTCTTTCTTCTCC
	AD18-BHL (*Xba*I)	GCGTCTAGAATTGGGCAAAGAAAGAATCTC
35Spr:cYFP-AtINP2	AD469 (*Pac*I)	CCCTTAATTAAAATGAGATTACAAGAGTTGGTT
	AD470 (*Xba*I)	5'-GCGTCTAGAACTAGATGATCCTGATCCCTT
AtINP1-pDONR207	AD326	AAAAAGCAGGCTAGAAAATGCCTTTCTCTTTC
	AD488	AGAAAGCTGGGTAGAGATTATTGGGCAAAGAA
	AD122	GGGGACAAGTTTGTACAAA AAA GCA GGC T
	AD123	GGGGACCACTTTGTACAAGAAAGCTGGGT
AtINP2-pDONR207	AD370	AAAAAGCAGGCTGATCCATGAGATTACAAGAG
	AD489	AGAAAGCTGGGTAAAGCTCACTAGATGATCCT
	AD122	GGGGACAAGTTTGTACAAAAAAGCAGGCT
	AD123	GGGGACCACTTTGTACAAGAAAGCTGGGT